Title

ECEF Position Accuracy and Reliability:Continent Scale Differential GNSS Approaches (Phase C Report)

Authors

Rahman, Farzana
Silva, Felipe
Jiang, Zeyi
et al.

Publication Date

2019-06-17

ECEF Position Accuracy and Reliability: Continent Scale Differential GNSS Approaches

Phase C Technical Report for Sirius XM

Farzana Rahman, Felipe Silva, Zeyi Jiang, and Jay A. Farrell
Department of Electrical and Computer Engineering, University of California, Riverside, 92521

June 17, 2019

Executive Summary

Many applications, including connected and autonomous vehicles, would benefit from navigation technologies that reliably achieve sub-meter position accuracy with high reliability on moving platforms. Real-time submeter Earth-referenced positioning accuracy has the potential to be achieved with high reliability on moving vehicles by using Global Navigation Satellite Systems (GNSS) if common-mode ranging error correction information is communicated to the vehicles. For successful commercial implementation, such correction information must be delivered on continental or global scales. The communication latency must be small enough to not significantly affect performance.

Phase A of this project presented a local differential correction computation methodology designed to be robust to latency and studied position estimation accuracy as a function of differential correction latency for stationary receivers [1]–[3]. The study showed that submeter accuracy at 95% probability was achievable when a sufficient number and diversity of satellites were available. This performance was robust to latency up to 600 seconds.

Phase B of this project studied position accuracy as a function of differential correction latency for moving receivers using two navigation algorithms. Both algorithms incorporated the local differential correction approach defined in Phase A [1]. The Position, Velocity, Acceleration (PVA) approach used only DGNSS data with a Kalman filter. The Inertial Navigation System (INS) approach used DGNSS and inertial measurement data within an extended Kalman filter. The study showed that both approaches achieved performance exceeding the SAE J2945 specification (1.5 meter horizontal accuracy and 3.0 meter vertical accuracy at 68%) [4] with PVA achieving 1 m horizontal accuracy at 90% and 2 m vertical accuracy at 95% and the INS approach using a consumer-grade IMU achieved 1 m horizontal accuracy at 98% and 2 m vertical accuracy at 95% [5].

This report summarizes the study and conclusions of Phase C. The main goals of Phase C were to investigate methods for implementing DGNSS corrections on a continental scale, to study the achievable accuracy, and to report on the factors determining the communication requirements. Section II presents a brief overview of GNSS systems. Section III states the problem that is of interest. Section IV reviews local DGNSS and presents an overview of continental scale network DGNSS approaches that are referred to as Wide Area DGNSS (WADGNSS). The overview includes discussion of WADGNSS, the models that it incorporates, the modeling agencies, and the existing data and model sources. Section V expands the discussion of WADGNSS approaches. It includes a discussion of communication requirements and points to Appendix A for a technical discussion of WADGNSS. Section VI summarizes the Precise Point Positioning (PPP) state estimation approaches that are experimentally investigated in Section VII. PPP methods are discussed in Section B. Section VIII concludes the report and lists the recommendations.

If Sirius XM decides to communicate GNSS common-mode ranging error correction information through its satellite communication channels, a main recommendation of this report (see Section V-A) is that Sirius XM collaborate with existing expert teams to obtain the WADGNSS correction information. Example sources of this information are in Table IV with an analysis of the bandwidth requirements for information distribution. After the common-mode ranging error correction information is available on Sirius XM receivers, that information can be organized using eqn. (7) into an L1 differential GNSS correction suitable for a user location in RTCM format for input to commercial GNSS receivers.

Using this approach, based on correction information accuracies stated in the literature (see Table V), horizontal position accuracy of 0.48 - 0.96 m should be achievable. Preliminary experiments performed in this project (see Section VII) have demonstrated horizontal position accuracies of 1.35 ± 0.48, 1.19 ± 0.41, and 0.47 ± 0.26 using PPP DGNSS and demonstrated horizontal position accuracies of 0.81 ± 0.21, 0.52 ± 0.25, and 0.43 ± 0.186 using PPP DGNSS aided INS.

This study focuses on single frequency, single constellation results. The availability of multiple constellations and multiple frequencies per constellation will facilitate estimation and compensation of ionospheric error, accommodation of outliers, and accommodation of multipath. It will also greatly increase the number of available measurements and the likelihood that the user has available a set of satellites with appropriate geometry to reliably achieve the performance specification.

CONTENTS

I. Introduction

Over the last several decades, Global Navigation Satellite Systems (GNSS) [6]–[9] have become dominant for personal and vehicular position determination for routing applications. For such applications, standard GNSS accuracy of about 10 m has typically been sufficient. The elements of the ranging error that contribute to this error budget are summarized in Table I. The horizontal position error is predicted by multiplying the user equivalent range error (UERE) by the horizontal dilution of position (HDOP).

TABLE I: Standard GNSS error budget.

Source	Error Budget, m
Ephemeris error	2
Satellite clock offset	2
Ionospheric time delay	3-7
Tropospheric error	1
Receiver noise	0.2
Multipath effect	1-2
UERE, rms	4-8
Horizontal Position Error, rms (HDOP = 1.5)	6-12

A new generation of applications (e.g., autonomous vehicles, connected vehicles, and driver's assistance [10]–[13]) are placing much stricter position accuracy and reliability specifications on navigation systems than was previously required. Specifically stated specifications (e.g., SAE J2945 [4]) require horizontal and vertical position accuracy of 1.5 m and 3 m with 68% probability, respectively. The FHWA, state DOTs, and auto manufacturers are investigating connected and autonomous highway vehicle applications which will benefit from real-time, Earth Centered Earth Fixed (ECEF) position estimates accurate to the sub-meter level at 95% probability. Pilot projects are ongoing in at least three locations [11]–[13]. The objectives of these projects include improving roadway network safety and throughput, while decreasing emissions impact.

Commonly cited local area differential GNSS (LADGNSS) position accuracy levels are 1-3 meters [14], but do not consider the effect of communication latency. The lower end of this range approaches the desired sub-meter specification, if this accuracy can be achieved with sufficient reliability and if it is not sensitive to DGNSS correction communication latency. Phases A and B of this project studied means to accommodate communication latency and studied the achievable positioning accuracy as a function of latency using LADGNSS. Phase A proposed and implemented a LADGNSS communication protocol [1]. Using that protocol, Phase B experimentally analyzed two state estimation approaches suitable for moving platforms [5]. The Position, Velocity, Acceleration (PVA) approach used LADGNSS data alone within a Kalman filter framework. The Inertial Navigation System (INS) approach used LADGNSS and inertial measurement data within an extended Kalman filter implementation. Both approaches demonstrated performance exceeding the SAE J2945 specification with PVA achieving 1 m horizontal at 90% and 2 m vertical accuracy at 95% and the INS approach using a consumer-grade IMU achieving 1 m horizontal at 98% and 2 m vertical accuracy at 95%. These methods demonstrated performance that was robust to communication latency of up to 500 second.

Since satellite communication methods are expected to incur latencies significantly less than 500 seconds, Phases A and B showed that it was feasible to surpass SAE J2945 positioning accuracy specifications even in the presence of expected satellite communication latencies. However local area DGNSS corrections are not feasible for continent scale DGNSS implementations.

This report summarizes the study and conclusions of the Phase C. The main goals of Phase C were to investigate methods for implementing DGNSS corrections on a continental scale, to study the achievable accuracy, and to report on the factors determining the communication requirements. Section II presents a brief overview of GNSS systems. Section III states the problem that is of interest. Section IV reviews local DGNSS and presents an overview of continental scale network DGNSS approaches that are referred to as Wide Area DGNSS (WADGNSS). The overview includes discussion of WADGNSS, the models that it incorporates, the modeling agencies, and the existing data and model sources. Section V expands the discussion of WADGNSS approaches. It includes a discussion of communication requirements and points to Appendix A for a technical discussion of WADGNSS. Section VI summarizes the estimation approaches that are experimentally investigated in Section VII. Section VIII concludes the report.

This study focuses on single frequency, single constellation results. The availability of multiple constellations and multiple frequencies per constellations will facilitate estimation and compensation of ionospheric error, accommodation of outliers, and accommodation of multipath. It will also greatly increase the likelihood that the user has available a set of satellites with appropriate geometry to reliably achieve the performance specification.

II. GNSS Background and Notation

This section introduces notation and GNSS measurement models. For additional information on GNSS, see [15]–[19].

GNSS receivers provide three measurements: pseudorange, carrier phase, and Doppler. At present, on inexpensive commercial receivers, these signals are available only on a single frequency referred to as L1. In the near-future, low-cost consumer receivers are expected to provide additional measurements from multiple constellations (e.g., GPS, GLONASS, Galileo, BeiDou) and at multiple frequencies (i.e., L1, L2, and L5 for GPS). The methods discussed herein generalize to multiple frequencies and constellations. Additional frequencies and multiple constellations will further enhance performance. For example, measurements at multiple frequencies will improve estimation of ionospheric delay. Multiple constellations and multiple frequencies will greatly increase the number of measurements allowing attenuation of multipath and outlier effects. This study focuses on users with access to L1 pseudorange and Doppler measurements from the GPS constellation.

A. Notation

To clearly distinguish between models and computations, this article will use two different symbols. The symbol $\doteq$ indicates

that the equation is a model. Models are used to analyze, understand, and physically interpret measurements, often with the goal of designing algorithms to estimate quantities that are of interest (e.g., position). The symbol $=$ indicates that an equation represents an actual algorithmic calculation.

When it is necessary to represent the actual, measured, and computed versions of a variable, x will represent the actual value, $\tilde{x}$ will represent the measured value, $\hat{x}$ will represent the computed or estimated value. Vector and matrix variables will be printed in bold font. For example, $\mathbf{p}^s$ represents the actual position vector for satellite s while $\hat{\mathbf{p}}^s$ represents the position vector for satellite s computed from the available ephemeris data.

B. GNSS Measurement Models

GNSS receivers track signals from satellites to provide pseudorange and phase measurements. For the GPS system, the measurement models are:

$$\begin{aligned}\rho^s_{r,L1} &= R(\mathbf{p}_r,\hat{\mathbf{p}}^s)+ct_r+cb_{r_{L1,\rho}}+M^s_{r,\rho 1}+\eta^s_{r,\rho 1}\\ &\quad -ct^s+E^s_r+I^s_{L1}+T^s-cb^s_{L1,\rho}, \qquad (1)\\ \rho^s_{r,L2} &= R(\mathbf{p}_r,\hat{\mathbf{p}}^s)+ct_r+cb_{r_{L2,\rho}}+M^s_{r,\rho 2}+\eta^s_{r,\rho 2}\\ &\quad -ct^s+E^s_r+I^s_{L2}+T^s-cb^s_{L2,\rho}, \qquad (2)\\ \phi^s_{r,L1} &= R(\mathbf{p}_r,\hat{\mathbf{p}}^s)+ct_r+cb_{r_{L1,\phi}}+\lambda_{L1}N^s_{r,L1}+M^s_{r,\phi 1}+\eta^s_{r,\phi 1}\\ &\quad -ct^s+E^s_r-I^s_{L1}+T^s-cb^s_{L1,\phi}, \qquad (3)\\ \phi^s_{r,L2} &= R(\mathbf{p}_r,\hat{\mathbf{p}}^s)+ct_r+cb_{r_{L2,\phi}}+\lambda_{L2}N^s_{r,L2}+M^s_{r,\phi 2}+\eta^s_{r,\phi 2}\\ &\quad -ct^s+E^s_r-I^s_{L2}+T^s-cb^s_{L2,\phi}. \qquad (4)\end{aligned}$$

where ρ represents pseudorange and ϕ represents carrier phase. The subscript r counts over the number of available receivers. The superscript s counts over the number of available satellites. The symbols L1 and L2 indicate the two GPS carrier frequencies and λ_{L1} and λ_{L2} are the corresponding carrier signal wavelengths. The symbols $N^s_{r,L1}$ and $N^s_{r,L2}$ represent the L1 and L2 integer ambiguities that arise from carrier phase tracking.

The desired information from these measurements is the range between the receiver position $\mathbf{p}_r$ and the satellite location $\mathbf{p}^s$

$$R(\mathbf{p}_r,\mathbf{p}^s)=\|\mathbf{p}_r-\mathbf{p}^s\|. \qquad (5)$$

Ephemeris error

$$E^s_r=R(\mathbf{p}_r,\mathbf{p}^s)-R(\mathbf{p}_r,\hat{\mathbf{p}}^s) \qquad (6)$$

arises because the actual satellite position $\mathbf{p}^s$ is not the same as the satellite position $\hat{\mathbf{p}}^s$ computed from the ephemeris data. In a perfect vacuum the range would equal the product of the time-of-travel and the speed-of-light in a vacuum. Because the underlying measurement is the time-of-travel of a signal sent by the satellite and detected by the receiver, the timing measurement is corrupted by the receiver clock bias ct_r, the satellite clock bias ct^s, and signal path delays within the receiver cb_{r_f} and satellite cb^s_f, where f is either L1 or L2. For the remaining terms: I^s_f represents ionospheric delay for frequency f, T^s represents tropospheric error, M^s_r represents multipath error, and $\eta^s_{r,*}\sim\mathcal{N}(0,R^s_*)$ is white random noise affecting the measurement, $*$ is may be replaced by "$\rho 1$", "$\rho 2$", "$\phi 1$", or "$\phi 2$". The error terms I^s_f and T^s arise because the signals travel through the Earth atmosphere, not a perfect vacuum.

The portions of this report that discuss estimation of the information necessary to compute *GNSS corrections* will assume availability of a continent-wide (or global) network of high-quality receivers and antennae, at locations known to centimeter or better accuracy, that are recording both pseudorange and carrier phase measurements on (at least) two frequencies.

The portions of this report that are concerned with position estimation assume a consumer grade antenna and receiver that provides pseudorange and Doppler on a single frequency. All experimental results herein use data only from GPS. Performance would be enhanced by using data from multiple GNSS's [20] or from multiple frequencies [21]. Availability of phase measurements could also greatly improve positioning accuracy if L1 integer ambiguities could be reliably estimated [14] or if convergence times of float estimates of integers [22] could be (greatly) reduced.

C. GNSS Measurement Errors

The L1 pseudorange measurement has 9 types of errors, (see [23], and Sections 1.2-1.3 of [14]). They can be classified into two categories:

- *Common-mode errors* (ephemeris, satellite clock bias, ionosphere, troposphere, satellite hardware bias) are common to all receivers in the same vicinity. In eqns. (1–4) the symbols representing these common-mode errors are in the second line of each equation.
- *Noncommon-mode errors* (receiver clock bias, receiver hardware bias, multipath, receiver noise) are different for each receiver.

Table I summarizes typical magnitudes for the various range error sources for standard GNSS, without differential corrections. The resulting horizontal position estimation accuracy does not achieve the desired specifications. Differential correction approaches (local DGNSS, network DGNSS, or PPP) aim to reduce the effects of the common-mode errors [24]–[27] on the position estimates.

III. Problem Statement

The main focus herein is DGNSS implementation approaches applicable to continent-wide or global scales. Specific topics of interest include: theoretically expected pseudorange accuracy; the extent to which state estimation algorithms can achieve the position accuracy and reliability specifications currently envisioned for driver assistance, connected vehicle, and autonomous vehicle applications [4]; and, communication requirements to ensure a time to first fix of a few seconds.

The discussion that follows will primarily focus on Network DGNSS [28]–[34] and precise point positioning (PPP) [35]–[38] methods.

IV. Continent Scale DGNSS Approaches

To enhance the accuracy of GNSS receiver position estimation, the user can compensate the common-mode errors using

correction information from external sources. At least three approaches exist to acquire this information: corrections from a local reference station can be directly applied (Local Area DGNSS); GNSS measurements from an array of reference stations could be used to estimate corrections for the local users (Network or Wide Area DGNSS); or, correction information estimated by national or global agencies could be used to construct corrections for the local user (Precise Point Positioning). These methods are discussed in more detail in the following subsections.

A. Local Area DGNSS Reference Station Network

Local Area DGNSS (LADGNSS) [14], [17] uses a reference GNSS receiver near the area of operations to compute a correction that is the sum of the common-mode errors at the reference location. This correction is communicated to roving receivers within a distance D of the reference location for which the correction is deemed to be accurate. This approach works well even for a large number of roving vehicles, each within distance D of the reference station, but does not scale well to large areas.

Let L and W represent the length and width of the continent-sized region for which the corrections are intended to apply. The number of required base stations would be on the order of $\left(\frac{L}{D}\right)\left(\frac{W}{D}\right)$. For example, for the lower forty eight US states $L = 2802$ and $W = 1650$ miles. Depending on the value selected for D, between 475-1850 base stations would be required. Each station would need to be robustly built, the antenna location surveyed, power and data communications installed, and the entire network maintained. The corrections from each station for each satellite would need to be communicated to the master station. If the communication medium provides a data stream across the continental US, then corrections from all reference stations for all satellites would be communicated to all users, who would then use the appropriate correction for the satellites in view at their location.

Such a network of GNSS receivers to implement a continental scale set of *local corrections* is not an efficient use of resources. It is also not reliable in the sense that the loss of any reference station would eliminate corrections applicable to the surrounding region. An alternative approach is discussed in the next section. It makes more efficient use of data, allowing a smaller network, and provides opportunities for enhanced integrity and reliability.

B. Network DGNSS

Wide-area DGNSS (WADGNSS) systems are designed to cover large, continent-sized regions [29]–[34], [39], [40]. They rely on data from a network of GNSS receivers dispersed across the region exploiting the spatial and time correlation characteristics of GNSS common-mode errors.

The WADGNSS concept includes a network of reference (or monitor) stations dispersed across the region of interest, one or more master stations (central processing sites), communication of data from the reference stations to the master station(s), and a data link to provide corrections from the master station(s) to users. Each reference station includes one or more GNSS receivers that measure pseudorange and carrier-phase for each frequency of the broadcast signals from all visible satellites. This data is provided to the master station(s). Wide-area DGNSS (WADGNSS) attempts to attain submeter-level position accuracy over the large region while using a fraction of the number of reference stations that a LADGNSS would require to attain the same accuracy within the same coverage region. The general approach, described in more detail in Appendix A, is to parameterize and estimate models for each component of the common-mode pseudorange error.

Satellite Ephemeris and Clock Error. The underlying cause of the ephemeris error in eqn. (6) is the satellite position error vector $(\mathbf{p}^s - \hat{\mathbf{p}}^s)$ that can be modeled by three parameters per satellite. Different reference stations are affected by different projections of this satellite position error vector onto their satellite line-of-sight vectors. Given four or more widely separated ground stations whose antenna positions are accurately known, accurate satellite position and clock error estimates can be achieved by combining the concept of a reverse-GNSS solution [28], [41] with sophisticated models to describe the motion of the GNSS satellites over time [42]. Such modeling is a standard method used for orbit determination for many satellite systems, including in the ground network for each GNSS constellation [39].

Ionospheric Delay. With multi-frequency measurements, each receiver at each epoch acquires one measurement per satellite of the slant ionospheric delay at the ionospheric pierce point for that satellite. Combining these slant delay measurements from all satellites and all base stations allows estimation of the parameters of an ionospheric vertical delay model [33], [34]. These vertical delay model parameters are broadcast to the user. The user equipment then computes a vertical ionospheric delay correction for each visible GNSS signal. The vertical delay correction is mapped into a slant delay correction based upon the elevation angle for each visible satellite.

Tropospheric Delay. Tropospheric delays are typically addressed through models (e.g., UNB3 [43], or Black's model [44]) employed at both the reference stations and the roving receiver.

Along with the items mentioned above the WADGNSS approach must calibrate various satellite and receiver hardware biases, and validate signal integrity.

C. Precise Point Positioning

Precise Point Positioning (PPP) methods are designed to utilize such wide-area network GNSS data products to compute more accurate user positions, without having to install and maintain a GNSS receiver network, master station, and estimation algorithms. Originally PPP methods were designed for post-processing using delayed network data products [35], [45], [46]. As these data products have become available in real-time, the interest has shifted to real-time PPP [36]–[38], [47]–[49].

After receiving parameters for the various error models, computing per satellite corrections, and applying all these corrections to its own pseudorange and phase measurements, the WADGNSS user equipment computes user position [39]. Approaches exist both for single and two frequency users. The PPP calculations are reviewed in Appendix B. Algorithms to use PPP corrections are presented in Section VI.

D. WADGNSS Modeling Agencies

There are various organizations using networks of GNSS stations that provide one or more component of the WADGNSS correction.

International GNSS Service (IGS): IGS is a data service designed to enable high precision positioning using GNSS. Centimeter accuracy has been demonstrated using integer-resolved carrier phase measurements from multi-frequency receivers [50], [51]. IGS uses data from about 300 permanent, continuously-operating reference stations distributed around the world [51]. IGS also has voluntary collaboration (for data sharing) with more than 200 organizations (e.g., JPL) in more than 80 countries. IGS provides differential corrections via the Internet in RTCM Space State Representation (SSR) message format [52]. It is fully functional for GPS and nearing full functionality for GLONASS.

Federal Aviation Association (FAA): FAA has established 38 base stations distributed over the continental US (CONUS) [14]. FAA was responsible for establishing an GPS augmentation system suitable for North-American users. Their existing correction service, called WAAS, is delivered to users via geostationary satellites that also provide additional ranging signals.

European Space Agency (ESA): ESA is responsible for establishing another GNSS augmentation system. ESA has established 40 ground stations across Europe, Africa and North America [14]. The ESA correction called EGNOS is delivered to users via geostationary satellites.

National Oceanic and Atmospheric Admin. (NOAA): NOAA is responsible for providing a near real-time ionospheric Total Electron Content (TEC) map for CONUS users. Approximately 60 base stations were installed and maintained by the agency to provide a data source for their system [53].

The described agencies provide DGNSS corrections accessible by public entities free of cost. There are also private agencies (e.g., Jet Propulsion Lab (JPL), Trimble) that provide their own functioning WADGNSS services for a user fee.

To illustrate the issues and challenges related to WADGNSS model parameter estimation the elements of one approach are described in Appendix A.

E. Existing WADGNSS Services

Numerous agencies have been working to establish network DGNSS services for almost 30 years [28]–[34], [40]. The established services can be categorized into two groups based on their communication channels: geostationary satellites or internet.

Satellite Based Augmentation Systems: SBAS is the generic name for any augmentation system that has implemented WADGNSS using satellites as communication channels [14], [54]. This augmentation service can provide ranging, integrity and correction information for users in different geographical locations. Some versions of SBAS are described below.

Wide Area Augmentation Service (WAAS): WAAS was developed by the US FAA to provide correction data for the GPS system [14]. The WAAS system is established based on two segments: (a) Ground segment, and (b) Space segment. The ground segment consists of all reference stations installed in CONUS and Hawaii. The reference station data is sent to the Master stations which compute the corrections and send them to Ground Uplink Stations (GUS), which then transmit to four satellites for rebroadcast to the users.

European Geostationary Overlay Service (EGNOS): This service was developed by ESA specifically for users with multi-GNSS receivers [14]. It provides correction services for the GPS, GLONASS and Galileo systems. The system has two segments: (a) ground segment with 40 base stations in Europe, Africa and North America, and (b) space segment with 3 geostationary satellites.

Multi-functional Satellite Augmentation Service (MSAS): This service was developed in Japan. It has 4 ground stations in Japan, Hawaii and Australia and 2 geosynchronous communication satellites [55].

Starfire: This is a private fee-based correction service. The system was developed by John Deere's NavCom and precision farming groups.

There are additional augmentation services that are not yet fully functional, including:

- *GPS Aided Geo Augmented Navigation System (GAGAN)* under development by India.
- *System for Differential Corrections and Monitoring (SDCM)* under development by Russia.

Internet Based Augmentation System: There are agencies working on computing network DGNSS services to be distributed via the Internet. For example, IGS has been working since 1994 to establish a real-time, precise GNSS positioning service [51]. The DGNSS correction would be delivered in RTCM SSR format [52], which consists of many message types containing information about precise orbit, clock, ionosphere, and satellite hardware biases.

F. Summary and Recommendation

GNSS systems are developing rapidly. In the very near future, consumer grade receivers will work with multiple GNSS systems (i.e., GPS, GLONASS, Galileo, and BeiDou) and multiple frequencies. Multi-GNSS and multi-frequency approaches provide better satellite signal availability, which has benefits for accuracy and reliability.

While satellite position error vectors, clock errors, and hardware biases are distinct for each system. The ionospheric and tropospheric portions of differential corrections apply to all GNSS

systems equally well and will be more accurately estimate in multi-GNSS and multi-frequency approaches due to more measurements, at more pierce points, and at more frequencies. For this reason, the number of unknowns to be estimated scales sublinearly with the number of GNSS systems or satellites.

Various agencies have established reliable GNSS reference station networks with robustly mounted and accurately surveyed antennas, reliable power and communications, and functioning maintenance plans. They also have established expertise and algorithms for verifying data validity, estimating the parameters of the models underlying the various portions of the GNSS correction, and verifying model integrity.

For these reasons, an entity (e.g., Sirius XM) seeking to use an existing satellite communication service to reliably deliver GNSS corrections to highway vehicles should collaborate with entities such as those listed above that already have the GNSS reference stations and WADGNSS algorithms in place. The organizations listed above would supply GNSS correction information (see Table IV) for delivery over the Sirius XM satellite communication channel. The Sirius XM receiver would use the received correction information to compute a correction for the collocated GNSS receiver using an equation such as eqn. (7).

V. WADGNSS Approach

This section describes data sources, methodology, and performance analysis related to implementing a WADGNSS service.

A. Data Sources

A major issue in the implementation of a WADGNSS network is the reliable real-time collection of GNSS data from multi-frequency receivers well-distributed across the USA.

Various private organizations (e.g., Trimble, JPL) have established and maintained an array of reference stations across the country, but the data from these reference stations are not accessible by public users. Alternatively, some public organizations (e.g., NOAA) have spatially distributed reference stations, but real-time free access is limited to only a few reference stations. Other public organizations (e.g. Plate Boundary Observatory (PBO), Scripps Orbit and Permanent Array Center (SOPAC)) provide freely accessible real-time data, but their spatial distribution does not currently cover the entire CONUS.

Table II summarizes information related to a few examples of available sources for reference station data in the CONUS. All the sources listed as public (including all NOAA sites) allow delayed downloading of data for post-processing.

TABLE II: Summary of Real-time Reference Station Networks.

Entities	Access	Free	Coverage
PBO	Public	Y	West coast
NOAA	Public Private	Y N	Limited USA
FRPN	Public	Y	Florida
Trimble	Private	N	USA
JPL	Private	N	Global

For an entity that desires to communicate real-time WADGNSS to automotive user there are various available approaches:

1) Compute its own WADGNSS information using data from:
   a) an entirely new network of reference stations installed and maintained by the entity or its contractor;
   b) existing free sources; or
   c) existing sources that charge a fee.
2) Collaborate with entities that already computed the components of WADGNSS corrections to distribute them through alternative communication channels.

Option 1 requires development of talent, methods, and algorithms. It also requires selection of a real-time reference station data delivery approach and may also run into intellectual property issues. Option 2 allows an entity with a well established expertise in data communications to focus on that strength, avoids intellectual property issues, avoids the need to acquire raw GNSS reference data in real-time, and relies on the well developed expertise of others for the estimation of model parameters.

B. WADGNSS Implementation Strategies

Given reference station data, WADGNSS modeling entities estimate model parameters for the three-dimensional ephemeris error and clock offset for each satellite, plus ionospheric time delay model parameters that can be communicated to user receivers in real-time. The algorithms may also estimate various additional quantities: reference receiver clock error, tropospheric delay, hardware biases, and carrier phase integer ambiguities. These quantities are not communicated to the user in real-time. The reference receiver clock error and integer ambiguities are nuisance parameters that must be estimated to achieve the specified accuracy in the desired model parameters, but are not themselves useful. The real-time tropospheric delay estimates are also discarded as they do not significantly enhance the user position estimation accuracy relative to the tropospheric model that is already used in the algorithm. The hardware delays are very slowly changing ($4.23e^{-4}$ ns/day or 0.13 mm/day), so they can be communicated at low rates (e.g., every 10 days).

The process can be summarized as follows: 1) reference stations at known locations collect GNSS pseudoranges and carrier phases (if available) from all satellites in view; 2) observations or processed observations (e.g., ionospheric-free pseudorange and ionospheric delay measurements (if available)) are sent to the master station; 3) the master station computes a state vector that includes the desired model parameters; 4) the model parameters are transmitted to users; 5) users calculate corrections using the model parameters and tropospheric model, then apply the corrections to their measured observations, resulting in improved navigation accuracy. Various WADGNSS techniques have been proposed in the literature [29]–[32], [41], [56], [57].

WADGNSS technique can be categorized according to the number of frequencies required for users and reference stations, which has implications for the estimation algorithm at the master station [32]:

TABLE III: Summary of WADGNSS Strategies.

Strategy	Number User Freqs.	Number reference Freqs.	Requirements
A	1	1	More reference stations than B and C
B	1	2	Fewer reference stations than A
C	2	2	More expensive user equipment Fewer reference stations than A

- **Strategy A**: This approach allows both the reference stations and users to employ single-frequency receivers. Because the reference station is single frequency it cannot provide ionospheric time measurements. This strategy uses an ionospheric model (e.g. Klobuchar model) to estimate and remove a portion of the ionospheric time delay from the reference station measurements prior to they are used by the master station. The master station estimates the three-dimensional ephemeris error vectors, the satellite clock errors and the reference receiver clock errors in one large filter using only the (ionospheric corrected) pseudorange measurements from all reference stations. The convergence time of the master station filter is stated as 2-4 hrs [32]. To use Strategy A for position estimation, requires the user to have an ionospheric model or Total Electron Content (TEC) map from another source. Position estimation accuracy is not stated in [32].
- **Strategy B**: This method requires the reference stations to use dual-frequency receivers, while the users can employ single-frequency (or two-frequency) receivers. With two frequencies, the reference station can construct measurements of ionospheric delay. Using these ionospheric delay measurements, allows a large estimation problem to be split into two smaller problems. Estimation of the vertical TEC map parameters using ionospheric delay measurements is one process. Estimation of the three-dimensional ephemeris error vectors, the satellite clock errors, and the reference station receiver clock errors is a separate process [32]. Relative to Strategy A, Strategy B has a lower computational load, uses fewer reference stations, and provides an vertical TEC map. For a rover using L1 carrier smoothed pseudorange measurement, [17] demonstrates position accuracy of 1.1 m.
- **Strategy C**: This method requires both reference stations and users to utilize dual-frequency receivers. In this case, ionospheric parameters do not need to be estimated in the master station, and as a result, only three-dimensional ephemeris error vectors and satellite clock errors are estimated. Compared to Strategy B, Strategy C has smaller computational load. It achieves the best accuracy among the aforementioned strategies, as this method removes ionospheric delay completely [31]. For a rover using L1 and L2 carrier smoothed pseudorange measurements, [32] demonstrates position accuracy of 0.71 m.

While Strategy C has the best reported accuracy and reduced computational load, the current project focuses on users with single frequency receivers; therefore, one implementation of Strategy B is reviewed in Appendix A.

C. Communication Requirements

In WADGNSS a master station computes and broadcasts to users the parameters for common-mode error models. This section analyzes the communication bandwidth requirements of WADGNSS Strategy B from the Master Station to the user equipment (i.e., the satellite channel). The summary is in Table IV. The analysis computes the required bit rate for the communication channel to send the data package.

There are a variety of suppliers of real-time WADGNSS correction parameters. For the analysis of communication requirements in Table IV, one example source is shown for each. The navigation message (i.e., broadcast ephemeris) is obtained from IGS-RTS. The precise orbit and clock corrections relative to the broadcast ephemeris are also obtained from IGS-RTS. The vertical TEC model parameters are provided by USTEC service. These items can be collected through the NTRIP protocol, packaged, and broadcast to Sirius receivers via satellites. Once the model parameters are available at the receiver, the receiver can compute corrections for each satellite applicable to the receiver location (see eqn. (7)), package the corrections in RTCM format, and supply the corrections to the GNSS receiver.

For each type of correction data, Column 3 shows the period T at which the message is sent from the source. This may be different from the period at which the data in the message changes. For example, the broadcast ephemeris changes every two hours, but is sent repeatedly every 5 seconds. Column 4 shows the average raw file size in kilo Bytes (KB). Columns 5-7 show the minimum, maximum, and average compressed file size using the gzip compression format. Column 8 shows the required bit rate to send each compressed file every T seconds. Column 9 shows the required bit rate to send each compressed file every 5 seconds, which would reduce the navigation time-to-first-fix (TTFF) from a cold-start to 5 seconds. The sum of the bit rates in Column 9 is 1.21 KB/s. The TTFF could be further reduced by sending each package more frequently. For example, sending the complete set of compressed data at 1 Hz would require approximately 6 KB/s of channel bandwidth.

D. Related Issues and Error Budget

A comparison of the user equivalent range error (UERE) that a user can achieve using Local or Wide-Area DGNSS is summarized in Table V [17]. The first column is the error type. The second column shows the stated accuracy to which each common-mode error type can be compensated using LADGNSS [17]. The third column shows the reported accuracy to which the WADGNSS model states the common-mode error can be corrected. The model source is listed in the fourth column. The accuracy stated for the orbit and clock corrections is from [37]. The accuracy stated for the ionospheric model (i.e., vertical TEC) is from [53]. The accuracy stated for tropospheric model is from [58]. The noncommon-mode errors' (multipath and receiver noise) nominal

TABLE IV: PPP Real-time Communication Requirements to the User

Type	Source	Update period, T, s	Raw Size, KB	Compressed Size, KB			Bitrate, KB/s	
			Avg	Min	Max	Avg	min(T,60) s	min(T,5) s
Broadcast ephemeris	IGS-RTS	5	19.8	5.07	5.1	5.09	0.09	0.09
Clock correction	IGS-RTS	5	1.52	0.33	0.35	0.34	0.07	0.07
Orbit correction	IGS-RTS	60	2.59	0.63	0.68	0.65	0.01	0.13
Ionosphere correction	USTEC	900	31.2	4.09	5.08	4.59	0.08	0.92

TABLE V: Local and Wide-Area Differential GNSS error budgets.

Error Type	LADGNSS Error Budget, m	WADGNSS Error Budget, m	Model Source
Ephemeris	0.4	0.05	IGS
Satellite clock	0.2	0.09	IGS
Ionospheric delay	0.5	0.40	USTEC
Tropospheric	0.3	0.05	UNB3M
Receiver noise	0.2	0.20	
Multipath	0.1	0.10	
UERE, rms	0.8	0.48	

values are obtained from [17]. Multipath error varies as a function of environment (e.g. urban, rural, open sky, obstructed view) and vehicle motion platform (stationary and moving). Receiver noise differs for both receiver and measurement type.

The UERE is converted to a horizontal position error by multiplication by the horizontal dilution of positions (HDOP), which for GPS with at least 6 satellites in view typically ranges from 1-2. Therefore, based on the last row of Table V, rms horizontal position error is predicted to be 0.8 - 1.6 m for LADGNSS and 0.48 - 0.96 m for WADGNSS.

VI. Estimation Approach

This section describes the PPP-based state estimation algorithms that were used for preliminary accuracy and reliability studies. The main ideas of the algorithms are described in the two previous reports [1], [5]. The main new aspect is that instead of using local DGNSS, the results herein use PPP corrections. As was the case for the studies in [1], the rover is stationary, but the algorithm parameters are tuned for dynamic conditions.

A. Precise Point Positioning (PPP)

The concept of precise point positioning was first introduced by Richard. J. Anderle [35] to enable high accuracy for single GNSS receivers that have access to WADGNSS data products (i.e., atmospheric models, precise satellite orbit and clock, satellite hardware biases) derived from external sources. PPP is reviewed in Appendix B.

With these WADGNSS data products, the user then can compute specific corrections for the user location. This allows computation of common-mode-error-free code and carrier phase measurements for estimating the receiver location without any nearby reference station. Most often, such PPP approaches use undifferenced ionosphere-free code and carrier phase observations from dual frequency receivers [45], [59]–[61], where centimeter accuracy is achievable if carrier phase ambiguities can be resolved. Alternatively, using floating integer estimates, decimeter accuracy can be achieved after a suitable convergence time (10's of minutes). The original PPP results were only feasible in post-processing due to latency in the required PPP data products. For on-vehicle applications, real-time results are needed from single frequency receivers without long convergence times.

Several services now provide real-time precise orbit, clock and ionospheric corrections (See Appendix B). These real-time data products enable the users to use PPP methods in real-time, if those data products can be communicated to the user receiver. The availability of ionospheric delay models creates the opportunity to utilize PPP for single frequency receivers. As a result, the current literature now contains different forms of single frequency real-time PPP techniques [36]–[38], [47], [62], [63].

For the PPP approach described in Appendix B, the common-mode ranging error correction information is formulated into a correction for the L1 signal on satellite s:

$$\hat{d}^s_{u,L1} = \hat{E}^{s_p} - c\hat{t}^{s_p} + \hat{I}^s_{L1} + \hat{T}^s - c\hat{b}^s_{L1,\rho}, \tag{7}$$

suitable for the users location. Then, the common-mode error compensated L1 pseudorange measurement $\tilde{\rho}^s_{u,L1}$ is computed as follows:

$$\tilde{\rho}^s_{u,L1} = \rho^s_{u,L1} - \hat{d}^s_{u,L1}, \tag{8}$$

where $\rho^s_{u,L1}$ is described by eqn. (1) with the subscript u denoting 'user'. The PPP common-mode error correction terms are:

- Precise orbit correction $\hat{E}^{s_p}$ from IGS-RTS that is computed using eqn. (38).
- Precise satellite clock correction $c\hat{t}^{s_p}$ from IGS-RTS that is computed using eqn. (40).
- Slant ionospheric delay for L1 users $\hat{I}^s_{L1}$ that is computed from USTEC's TEC map using eqn. (42).
- Slant tropospheric delay $\hat{T}^s$ is computed using eqn. (43) where the UNB3M model provides d^s_{dry}, d^s_{wet}, M^s_{dry}, and M^s_{wet}.
- Satellite hardware bias for the L1 user $c\hat{b}^s_{L1,\rho}$ that is computed using eqn. (44).

The measurement model for $\tilde{\rho}^s_{u,L1}$ is:

$$\tilde{\rho}^s_{u,L1} \doteq R(\mathbf{p}_u, \hat{\mathbf{p}}^s) + ct_u + cb_{u_{L1,\rho}} + M^s_{u,\rho} + \gamma^s_{u,\rho}. \tag{9}$$

The correction $\hat{d}^s_{u,L1}$ in eqn. (7) is suitable for communicating via the commercial GNSS receivers, for example using message 1004 of RTCM Version 3.1 [24], [25].

B. Position Estimation Algorithms

Section VII will study performance using three algorithms:

PPP-LS: This defines the state vector as

$$\mathbf{x}(t) = [\mathbf{p}^T, t_r]^T \in \Re^4$$

and solves each epoch of data separately using Least Squares (LS) with L1 PPP pseudorange measurements. These results are point-wise, without any filtering.

PPP-PVA: This defines the state vector as

$$\mathbf{x}(t) = [\mathbf{p}^T, \mathbf{v}^T, \mathbf{a}^T, \mathbf{s}_v^T]^T \in \Re^{9+m}$$

and estimates the state using a linear Kalman Filter (KF) with single-differenced (between satellites) PPP L1 pseudorange and Doppler measurements.

PPP-INS: This defines the state vector as

$$\mathbf{x}(t) = [\mathbf{p}^T, \mathbf{v}^T, \mathbf{q}^T, \mathbf{b}_a^T, \mathbf{b}_g^T, \mathbf{s}_v^T]^T \in \Re^{16+m}$$

and estimates the state using an extended Kalman Filter (KF) with single-differenced (between satellites) PPP L1 pseudorange and Doppler measurements. The IMU data is artificially generated to have the characteristics of a consumer-grade IMU (i.e., ADIS16360) (see appendix of [5]).

Each algorithm processes the set of GNSS measurements ($k = 1,\ldots,N_d$) incrementally, as if they were occurring in real-time, to estimate the state vector at each time k. The state variable s_v is a vector with one element per satellite. This state is augmented to account for multipath and residual atmospheric errors.

The symbol $\hat{\mathbf{p}}_k^a$ denotes the position estimated at time k for algorithm a, where $a = 1$ for PPP-LS, $a = 2$ for PPP-PVA, and $a = 3$ for PPP-INS.

C. Accuracy Metric

One of the metrics for comparison of algorithms will be the norm of the horizontal position error at time k. For scenario a this metric is computed as

$$e_{h_k}^a = \left\| \begin{bmatrix} 1 & 0 & 0 \\ 0 & 1 & 0 \end{bmatrix} (\mathbf{p}_r - \hat{\mathbf{p}}_k^a) \right\| \tag{10}$$

where p_r is the receiver antenna's ground truth position. The ground truth position is known to centimeter accuracy from other methods. This equation assumes that the position vector is represented in the North-East-Down navigation frame. The vertical position error $e_{v_{k,l}}^a$ is defined as

$$e_{v_k}^a = \begin{bmatrix} 0 & 0 & 1 \end{bmatrix} (\mathbf{p}_r - \hat{\mathbf{p}}_k^a).$$

The results and performance analysis is presented in Section VII.

VII. Experimental Results

This section presents experimental results for positioning performance using the three PPP algorithms defined in Section VI. A goal is to analyze the ability to satisfy a one-meter accuracy specification.

TABLE VI: Dataset Description.

Base Station	Location	Receiver Name	Antenna Type	Data Length, s
BRMU	Bermuda	LEICA GRX1200GGPRO	JAVRINGANT DM + None	3600
HNTP	Maryland	LEICA GRX1200GGPRO	LEIAX1202GG + None	3040
QUIN	California	JAVAD TRE 3 DELTA	ASH701945E M + SNOW	3100

A. PPP Datasets

The experimental analysis will use L1 pseudorange and Doppler measurements. Carrier phase measurements were not directly used because integer resolution is not reliable for single-frequency receivers and the float solution require tens of minutes to converge.

To evaluate the consistency of the PPP results, experiments were performed using spatially separated datasets. Each dataset is from a stationary reference antenna for which the ground truth position is known. Table VI summarizes key information about each dataset. The first column displays the name of the reference station in the CORS network, which will also be used as the name of the dataset. The second column states the general location of the reference station. The third column states the receiver brand and model. The fourth column states the antenna type brand and model. The fifth column states the length of the dataset in seconds. All of these datasets were acquired using ftp in Rinex 2.11 format for the same time: date-March 12, 2019 and time-7:00 pm in Pacific time-zone. The PPP data to compute real-time corrections was acquired from the sources listed in Table IV for the same date and time. The 200 Hz IMU data for the PPP-INS algorithm was artificially generated to have consumer grade sensor characteristics (see the Appendix B of [5]).

B. Positioning Accuracy

Fig. 1 shows histograms of $e_{h_k}^a$ as defined in eqn. (10) for the three datasets described in Section VII-A and for each algorithm defined in Section VI-B. Each column shows the histogram of a given algorithm for all three datasets. Each row shows the histogram of all three algorithms for a given dataset. The performance improves as the algorithm improves (INS is better than PVA which is better than LS).

Statistics quantifying the performance of each algorithm are summarized in Table VII. Each row of tables corresponds to one of the datasets listed in Table VI. The left column of tables contains statistics for the horizontal position error. The right column of tables contains statistics for the vertical position error. The statistics in each table are as follows. Column 1 shows the algorithm number a and name. Column 2 displays the mean norm of the position error. Column 3 contains the standard deviation of the norm of the position error. Column 4 shows the maximum value of the norm of the position error. Columns 5 and 6 report the percentage of samples for which the norm of the positioning error is less than the accuracy specified in the column header.

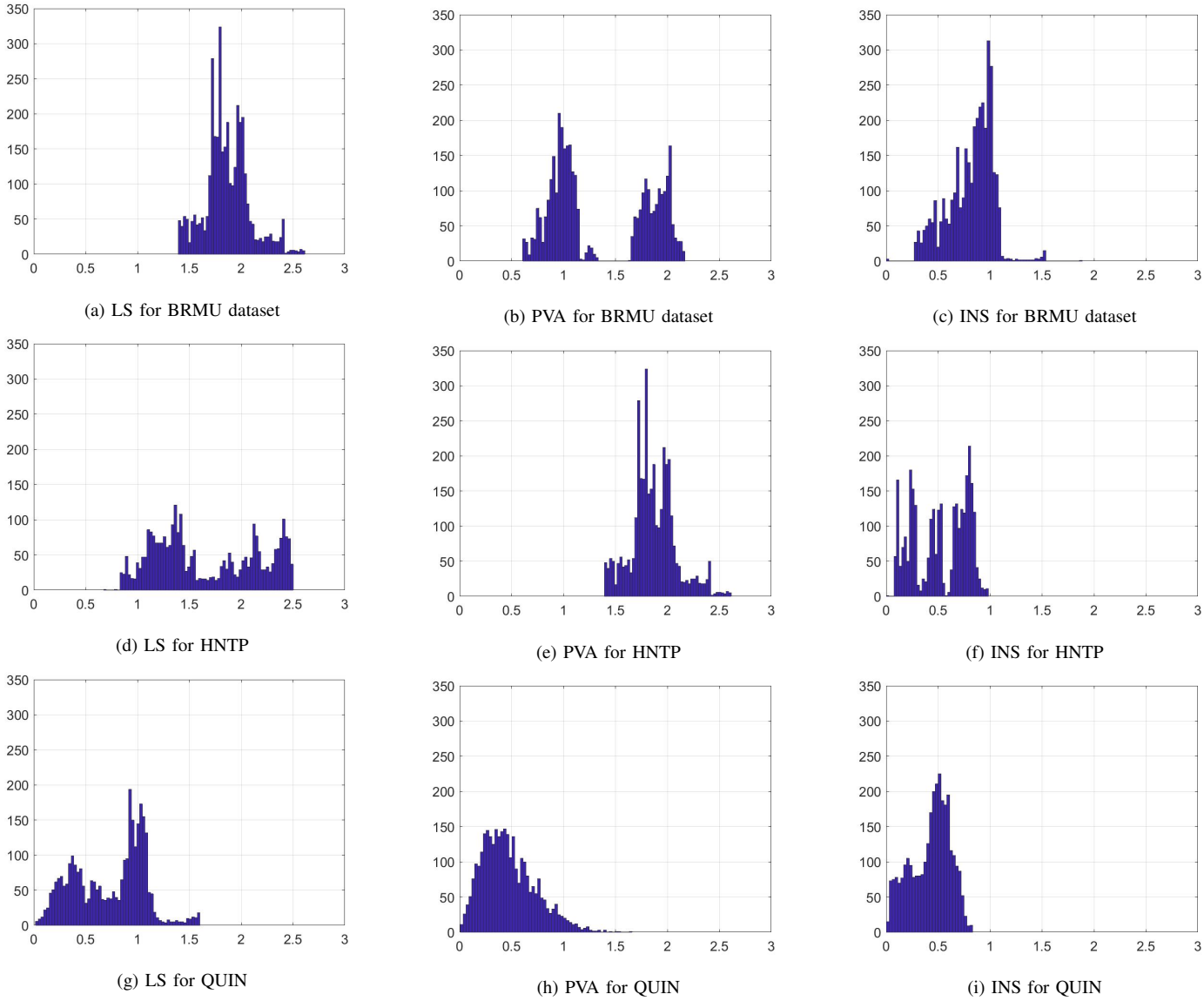

(a) LS for BRMU dataset (b) PVA for BRMU dataset (c) INS for BRMU dataset

(d) LS for HNTP (e) PVA for HNTP (f) INS for HNTP

(g) LS for QUIN (h) PVA for QUIN (i) INS for QUIN

Fig. 1: Histogram plots of the horizontal position error for the datasets described in Table VI.

Both the histogram and the tables show that, for the HNTP and QUIN datasets, the INS results exceed the SAE specification [4]. The INS, which has more information, performs better than LS and PVA approaches. The INS performance is expected to carryover to datasets for moving platforms, because the job of the IMU/INS is to remove the mean motion of the platform. The performance of the PVA approach may be distinct for each moving platform dataset, depending on the extend to which the platform motion matches the design assumptions of the PVA estimation approach [64].

VIII. Conclusions

This report concludes a three phase study performed by the University of California Riverside for Sirius XM.

Phase A studied the achieveable accuracy of local area differential corrections as a function of communication latency. A main question was whether the tens of seconds of latency expected in satellite communication links would adversely affect positioning accuracy. Because the conclusion would not be affected by user motion, this Phase A used data from stationary antennae. The study showed that submeter accuracy at 95% probability was achievable when a sufficient number and diversity of satellites were available. This performance was robust to latency up to 600 seconds [1]–[3].

Phase B extended the study of accuracy versus differential correction communication latency to moving platforms using two different algorithms: a PVA model using only differential GPS data and a differential GPS aided INS approach that also

TABLE VII: Positioning Performance of the Algorithms Defined in Section VI.

(a) Horizontal Error Statistics for BRMU dataset.

Scenario	Mean	Std. Dev	Max	Prob.	
				$e^a_{h_{k,0}} < 1m$	$e^a_{h_{k,0}} < 2m$
1. LS	1.86	0.21	2.61	0	77
2. PVA	1.35	0.48	2.16	34	89
3. CG-INS	0.81	0.21	1.88	82	100

(b) Vertical Error Statistics for BRMU dataset.

Scenario	Mean	Std. Dev	Max	Prob.	
				$e^a_{v_{k,0}} < 2m$	$e^a_{v_{k,0}} < 3m$
1. LS	2.85	2.33	5.41	31	39
2. PVA	4.18	0.87	6.56	0	10
3. CG-INS	5.51	1.26	8.04	0.08	0.08

(c) Horizontal Error Statistics for HNTP dataset.

Scenario	Mean	Std. Dev	Max	Prob.	
				$e^a_{h_{k,0}} < 1m$	$e^a_{h_{k,0}} < 2m$
1. LS	1.67	0.49	2.50	6	65
2. PVA	1.19	0.41	2.24	45	96
3. CG-INS	0.52	0.25	0.98	100	100

(d) Vertical Error Statistics for HNTP dataset.

Scenario	Mean	Std. Dev	Max	Prob.	
				$e^a_{v_{k,0}} < 2m$	$e^a_{v_{k,0}} < 3m$
1. LS	1.37	0.51	2.40	85	100
2. PVA	1.70	0.47	2.67	70	100
3. CG-INS	0.03	0.63	1.21	100	100

(e) Horizontal Error Statistics for QUIN dataset.

Scenario	Mean	Std. Dev	Max	Prob.	
				$e^a_{h_{k,0}} < 1m$	$e^a_{h_{k,0}} < 2m$
1. LS	0.73	0.34	1.60	74	100
2. PVA	0.47	0.26	3.19	96	100
3. CG-INS	0.43	0.18	0.83	100	100

(f) Vertical Error Statistics for QUIN dataset.

Scenario	Mean	Std. Dev	Max	Prob.	
				$e^a_{v_{k,0}} < 2m$	$e^a_{v_{k,0}} < 3m$
1. LS	4.12	2.60	8.47	30	37
2. PVA	0.80	1.02	4.05	93	99
3. CG-INS	0.84	0.61	2.71	95	100

incorporated inertial measurements. The study showed that both approaches achieved performance exceeding the SAE J2945 specification (1.5 meter horizontal accuracy and 3.0 meter vertical accuracy at 68%) [4] with PVA achieving 1 m horizontal accuracy at 90% and 2 m vertical accuracy at 95% and the INS approach using a consumer-grade IMU achieved 1 m horizontal accuracy at 98% and 2 m vertical accuracy at 95% [5].

This report concludes Phase C. The main goals of Phase C were to investigate differential GNSS correction approaches suitable for continental scale implementations. The main recommendations of the study are:

1) Sirius should not implement its own network of GNSS reference stations. Such networks already exist, are well maintained, and the data should be available for a fee if Sirius chooses to implement its own WADGNSS algorithms. See Appendix A.
2) Sirius should not implement its own WADGNSS algorithms. Various entities world wide have decades of expertise and intellectual property. Some of these entities should be willing to collaborate to attain distribution channels directly to highway vehicles.
3) Sirius should broadcast WADGNSS data products. Example sources of this information are in Table IV with an analysis of the bandwidth requirements for information distribution. Using eqn. (7) and a Precise Point Positioning approach similar to that in Appendix B, the Sirius receiver could package those data products into an RTCM format for use immediately by any commercial receiver.
4) Sirius should also broadcast the GPS navigation message. This can significantly decrease the time-to-first-fix for a cold starting receiver.

This approach works for the L1 GPS receivers currently available. It extends to other GNSS systems and multiple GNSS frequencies with only minor changes in the communication requirements. The availability of multiple constellations and multiple frequencies per constellation will greatly increase the number of available measurements and the likelihood that the user has available a set of satellites with appropriate geometry to reliably achieve the performance specification.

Using the example approach described herein, based on the reported accuracies in the literature, horizontal position accuracy of 0.48 - 0.96 m should be achievable. Preliminary experiments performed during this project have demonstrated horizontal position accuracies of 1.35 ± 0.48, 1.19 ± 0.41, and 0.47 ± 0.26 using PPP DGNSS and demonstrated horizontal position accuracies of 0.81 ± 0.21, 0.52 ± 0.25, and 0.43 ± 0.186 using PPP DGNSS aided INS.

IX. Acknowledgement

The authors greatly appreciate the grant from Sirius XM that made this research and report possible. The statements herein are those of the authors and should not be interpretted as the opinions of the research sponsor.

REFERENCES

[1] F. Rahman, E. Aghapour, and J. A. Farrell, "ECEF Position Accuracy and Reliability in the Presence of Differential Correction Latency: Phase A Technical Report," University of California, Riverside, Tech. Rep., October, 2018. [Online]. Available: escholarship.org/uc/item/38d3h08w

[2] ——, "ECEF Position Accuracy and Reliability in the Presence of Differential Correction Latency," *IEEE/ION PLANS*, pp. 583–588, 2018.

[3] E. Aghapour, F. Rahman, and J. A. Farrell, "Risk-averse performance-specified state estimation," *IEEE/ION PLANS*, pp. 627–633, 2018.

[4] Anonymous, "On-Board System Requirements for V2V Safety Communications," Society of Automotive Engineers, Tech. Rep., March, 2016. [Online]. Available: https://saemobilus.sae.org/content/j2945/1_201603

[5] F. Rahman and J. A. Farrell, "ECEF Position Accuracy and Reliability in the Presence of Differential Correction Latency: Phase B Technical Report," University of California, Riverside, Tech. Rep., June, 2019. [Online]. Available: escholarship.org/uc/item/135578mw

[6] G. Blewitt, "Basics of the GPS Technique: Observation Equations," *Geodetic Applications of GNSS*, pp. 10–54, 1997.

[7] C. Shuxin, Y. Wang, and C. Fei, "A study of differential GNSS positioning accuracy," *3rd Int. Conf. on Microwave and Millimeter Wave Tech.*, pp. 361–364, 2002.

[8] P. Misra and P. Enge, "Special issue on global positioning system," *Proc. of the IEEE*, vol. 87, no. 1, pp. 3–15, 1999.

[9] B. Hofmann-Wellenhof, H. Lichtenegger, and J. Collins, *"Global Positioning System: Theory and Practice"*. Springer Science & Business Media, 2012.

[10] C. Basnayake, M. Joerger, and J. Auld, "Safety-Critical Positioning for Automotive Applications: Lessons from Civil Aviation," Inside GNSS, Tech. Rep., November, 2016. [Online]. Available: http://insidegnss.com/assets/webinar/201611/Inside-GNSS-Webinar_Safety-Critical-Positioning-for-Automotive-20161103.pdf

[11] F. M. Kitchener, T. English *et al.*, "Connected Vehicle Pilot Deployment Program Phase 2, Data Management Plan-Wyoming." USDOT, Tech. Rep., April, 2017. [Online]. Available: https://transportationops.org/publications/connected-vehicle-pilot-deployment-program-phase-2-data-management-plan-wyoming-dot

[12] S. Cadzow *et al.*, "Connected Vehicle Pilot Deployment Program Phase 2: Data Privacy Plan-New York City." USDOT, Tech. Rep., December, 2016. [Online]. Available: https://rosap.ntl.bts.gov/view/dot/32311

[13] S. Johnson, L. Rolfes *et al.*, "Connected Vehicle Pilot Deployment Program Phase II Data Privacy Plan-Tampa (THEA)." USDOT, Tech. Rep., February, 2017. [Online]. Available: https://rosap.ntl.bts.gov/view/dot/32763

[14] P. Teunissen and O. Montenbruck, *Handbook of Global Navigation Satellite Systems*. Springer, 2017.

[15] M. S. Braasch and A. Van Dierendonck, "GPS receiver architectures and measurements," *Proc. of the IEEE*, vol. 87(1), pp. 48–64, 1999.

[16] P. Misra and P. Enge, *Global Positioning System: Signals, Measurements and Performance*, 2nd ed. Massachusetts: Ganga-Jamuna Press, 2006.

[17] B. W. Parkinson, P. Enge, P. Axelrad, and J. J. Spilker Jr, *Global positioning system: Theory and applications*. American Inst. of Aeronautics and Astronautics, 1996.

[18] J. A. Farrell, *"Aided Navigation: GNSS with High Rate Sensors"*. McGraw-Hill Inc, 2008.

[19] P. Enge, "The global positioning system: Signals, measurements, and performance," *Int. J. of Wireless Info. Net.*, vol. 1(2), pp. 83–105, 1994.

[20] P. F. de Bakker and C. C. Tiberius, "Real-time multi-GNSS single-frequency precise point positioning," *GPS Solutions*, vol. 21(4), pp. 1791–1803, 2017.

[21] Y. Lou, F. Zheng, S. Gu, C. Wang, H. Guo, and Y. Feng, "Multi-GNSS precise point positioning with raw single-frequency and dual-frequency measurement models," *GPS Solutions*, vol. 20(4), pp. 849–862, 2016.

[22] C. Cai, Y. Gong, Y. Gao, and C. Kuang, "An approach to speed up single-frequency PPP convergence with quad-constellation GNSS and GIM," *Sensors*, vol. 17(6), p. 1302, 2017.

[23] G. Lachapelle, "GNSS observables and error sources for kinematic positioning," *Kinematic Systems in Geodesy, Surveying, and Remote Sensing*, pp. 17–26, 1991.

[24] Anonymous, "RTCM 10403.2: Differential GNSS (Global Navigation Satellite Systems) Service," Radio Technical Commission for Maritime Services, Tech. Rep., February, 2013.

[25] ——, "10403.1 for Differential GNSS (Global Navigation Satellite Systems) Services-Version 3," Radio Technical Commission for Maritime Services, Tech. Rep., 2006.

[26] P. K. Enge, R. M. Kalafus, and M. F. Ruane, "Differential operation of the global positioning system," *IEEE Comm. Mag.*, vol. 26(7), pp. 48–60, 1988.

[27] P. Teunissen, "Differential GPS: Concepts and Quality Control," *Netherlands Institution of Navigation, Amsterdam*, 1991.

[28] C. Kee, B. W. Parkinson, and P. Axelrad, "Wide area differential GPS," *Navigation*, vol. 38(2), pp. 123–145, 1991.

[29] C. Kee and B. W. Parkinson, "Algorithms and implementation of wide area differential GPS," *Proc. ION GPS*, 1992.

[30] ——, "High accuracy GPS positioning in the continent: Wide area differential GPS," *Proc. Differential Satellite Navigation Systems*, 1993.

[31] ——, "Wide area differential GPS as a future navigation system in the U.S." *IEEE Proc. Position Location and Navigation Symposium*, 1994.

[32] ——, "Wide area differential GPS (WADGPS): Future navigation system," *IEEE T. Aero. Elec. Sys.*, vol. 32(2), pp. 795–808, 1996.

[33] P. Enge, T. Walter, S. Pullen, C. Kee, Y.-C. Chao, and Y.-J. Tsai, "Wide area augmentation of the global positioning system," *Proc. of the IEEE*, vol. 84(8), pp. 1063–1088, 1996.

[34] A. Mannucci, B. Wilson, D. Yuan, C. Ho, U. Lindqwister, and T. Runge, "A global mapping technique for GPS-derived ionospheric total electron content measurements," *Radio Science*, vol. 33(3), pp. 565–582, 1998.

[35] R. J. Anderle, "Point positioning concept using precise ephemeris," *Satellite Doppler Positioning*, pp. 47–75, 1976.

[36] G. Krzan and P. Przestrzelski, "GPS/GLONASS precise point positioning with IGS real-time service products," *Acta Geodyn. Geomater*, vol. 13(1), pp. 69–81, 2016.

[37] S. Choy, "Investigation into the accuracy of single frequency precise point positioning (PPP)," *PhD Thesis. School of Mathematical and Geospatial Sciences, RMIT University*, 2009.

[38] W. Liu, "Positioning performance of single-frequency GNSS receiver using Australian regional ionospheric corrections," *Queensland University of Technology*, 2016.

[39] E. D. Kaplan and C. J. Hegarty, *Understanding GPS/GNSS - Principles and Applications*. Artech House, 2018.

[40] C. Kee, B. W. Parkinson, and P. Axelrad, "Wide area differential GPS," *Navigation*, vol. 38(2), pp. 123–145, 1991.

[41] A. Brown, "Extended Differential GPS," *Navigation*, vol. 36(3), pp. 265–285, 1989.

[42] J. Ceva, W. Bertinger, R. Mullerschoen, Y. T., and B. Parkinson, "Incorporation of orbital dynamics to improve wide area differential GPS," *Proc. ION GPS*, 1995.

[43] P. Collins, R. B. Langley, and J. LaMance, "Limiting Factors in Tropospheric Propagation Delay Error Modelling for GPS Airborne Navigation," *Proc. ION Annual Meeting*, 1996.

[44] H. D. Black, "An easily implemented algorithm for the tropospheric range correction," *J. Geophys. Res.*, vol. 83(B4), pp. 1825–1828, 1978.

[45] J. Zumberge, M. Heflin, D. Jefferson, M. Watkins, and F. Webb, "Precise point positioning for the efficient and robust analysis of GPS data from large networks," *Jour. of Geophysical Research: Solid Earth*, vol. 102(B3), pp. 5005–5017, 1997.

[46] S. Bisnath and Y. Gao, "Current state of precise point positioning and future prospects and limitations," *Proc. of International Association of Geodesy Symposia:Observing our Changing Earth, Springer*, pp. 615–623, 2009.

[47] R. J. van Bree and C. C. Tiberius, "Real-time single-frequency precise point positioning: accuracy assessment," *GPS Solutions*, vol. 16(2), pp. 259–266, 2012.

[48] J. Geng, F. N. Teferle, X. Meng, and A. Dodson, "Towards PPP-RTK: Ambiguity resolution in real-time precise point positioning," *Advances in Space Research*, vol. 47(10), pp. 1664–1673, 2011.

[49] D. Laurichesse, "The CNES Real-time PPP with undifferenced integer ambiguity resolution demonstrator," *Proceedings of the ION GNSS*, pp. 654–662, 2011.

[50] Y. Gao and K. Chen, "Performance analysis of precise point positioning using real-time orbit and clock products," *Positioning*, vol. 1(8), p. 0, 2004.

[51] J. Kouba, "A guide to using International GNSS Service (IGS) products," IGS Central Bureau, Pasadena, Tech. Rep., 2009. [Online]. Available: http://igscb.jpl.nasa.gov/igscb/resource/pubs/GuidetoUsingIGSProducts.pdf

[52] T. Hadas and J. Bosy, "IGS RTS precise orbits and clocks verification and quality degradation over time," *GPS Solutions*, vol. 19(1), pp. 93–105, 2015.

[53] E. Araujo-Pradere, T. Fuller-Rowell, P. Spencer, and C. Minter, "Differential validation of the US-TEC model," *Radio Science*, vol. 42(3), 2007.

[54] L. Li, C. Jia, L. Zhao, J. Cheng, J. Liu, and J. Ding, "Real-time single frequency precise point positioning using SBAS corrections," *Sensors*, vol. 16(8), p. 1261, 2016.
[55] A. Shimamura, "MSAS (MTSAT satellite-based augmentation system) project status," *Air & Space Europe*, vol. 1(2), pp. 63–67, 1999.
[56] P. V. W. Loomis, R. P. Denaro, and P. Saunders, "Worldwide differential GPS for space shuttle landing operations," *IEEE Position Location and Navigation Symp.*, 1990.
[57] V. Ashkenazi, C. J. Hill, W. Y. Ochieng, and J. Nagle, "Wide-area differential GPS: A performance study," *Navigation*, vol. 40(3), no. 3, pp. 297–319, 1993.
[58] R. Leandro, M. Santos, and R. B. Langley, "UNB neutral atmosphere models: development and performance," *Proc. of ION NTM*, vol. 52(1), pp. 564–73, 2006.
[59] J. Kouba and P. Héroux, "GPS Precise Point Positioning Using IGS Orbit Products, geodetic Survey Division," *Natural Resources Canada*, vol. 615, 2000.
[60] ——, "Precise point positioning using IGS orbit and clock products," *GPS solutions*, vol. 5(2), pp. 12–28, 2001.
[61] P. Teunissen and A. Khodabandeh, "Review and principles of PPP-RTK methods," *Jour. of Geodesy*, vol. 89(3), pp. 217–240, 2015.
[62] C. Cai, Z. Liu, and X. Luo, "Single-frequency ionosphere-free precise point positioning using combined GPS and GLONASS observations," *The Jour. of Navigation*, vol. 66(3), no. 3, pp. 417–434, 2013.
[63] M. Kim and K.-D. Park, "Development and positioning accuracy assessment of single-frequency precise point positioning algorithms by combining GPS code-pseudorange measurements with real-time SSR corrections," *Sensors*, vol. 17(6), p. 1347, 2017.
[64] F. Rahman and J. A. Farrell, "Earth-Centered Earth-Fixed (ECEF) Vehicle State Estimation Performance," *CCTA, in press*, 2019.
[65] B. D. Wilson and A. J. Mannucci, "Instrumental biases in ionospheric measurements derived from GPS data," *Proc. ION*, 1993.
[66] E. Sardón, A. Rius, and N. Zarraoa, "Estimation of the transmitter and receiver differential biases and the ionospheric total electron content from Global Positioning System observations," *Radio Science*, vol. 29(3), pp. 577–586, 1994.
[67] M. H. Pajares, J. M. Juan, and J. Sanz, "New approaches in global ionospheric determination using ground GPS data," *J. Atmos. Sol. - Terr. Phy.*, vol. 61(1), no. 1, pp. 1237–1247, 1999.
[68] A. Tetewsky, J. Ross, A. Soltz, N. Vaughn, J. Anszperger, C. O'Brien, D. Graham, D. Craig, and J. Lozow, "Making sense of inter-signal corrections: accounting for GPS satellite calibration parameters in legacy and modernized ionosphere correction algorithms," *Inside GNSS*, vol. July-August(1), pp. 37–48, 2009.
[69] N. Jakowski, C. Mayer, M. M. Hoque, and V. Wilken, "Total electron content models and their use in ionosphere monitoring," *Radio Science*, vol. 46(RS0D18), pp. 1–11, 1994.
[70] M. S. Grewal, A. P. Andrews, and C. G. Bartone, *"Global Navigation Satellite Systems, Inertial Navigation & Integration"*. John Wiley & Sons, 2013.
[71] D. Odijk and L. Wanninger, *Springer Handbook of Global Navigation Satellite Systems*. Springer, 2017.
[72] B. Park, C. Lim, Y. Yun, E. Kim, and C. Kee, "Optimal divergence-free Hatch filter for GNSS single-frequency measurement," *Sensors*, vol. 17(3), p. 448, 2017.
[73] L. Dyrud, A. Jovancevic, A. Brown, D. Wilson, and S. Ganguly, "Ionospheric measurement with GPS: Receiver techniques and methods," *Radio Science*, vol. 43(6), pp. 1–11, 2008.
[74] D. Sunehra, "TEC and Instrumental Bias Estimation of GAGAN Station Using Kalman Filter and SCORE Algorithm," *Positioning*, vol. 7(1), p. 41, 2015.
[75] R. R. Hatch, "The synergism of GPS code and carrier measurements," *Proc. 3rd International Geodetic Symp. on Satellite Doppler Positioning*, 1982.
[76] C. Goad, *Global Positioning System: Theory and Applications*. AIAA, 1996, ch. Surveying with the Global Positioning System.
[77] H. Hopfield, "Two-quartic tropospheric refractivity profile for correcting satellite data," *Jour. of Geophy. Research*, vol. 74(18), pp. 4487–4499, 1969.
[78] J. Saastamoinen, "Atmospheric correction for the troposphere and stratosphere in radio ranging satellites," *The Use of Artificial Satellites for Geodesy*, pp. 247–251, 1972.
[79] H. Zhang, Y. Yuan, W. Li, Y. Li, and Y. Chai, "Assessment of three tropospheric delay models (IGGtrop, EGNOS and UNB3m) based on precise point positioning in the Chinese region," *Sensors*, vol. 16(1), p. 122, 2016.
[80] M. B. El-Arini, P. A. O'Donnell, P. Kellam, J. A. Klobuchar, T. C. Wisser, and P. H. Doherty, "The FAA wide area differential GPS (WADGPS) static ionospheric experiment," *Proc. ION National Technical Meeting*, 1993.
[81] J. A. Klobuchar, P. H. Doherty, and M. B. El-Arini, "Potential ionospheric limitations to Wide Area Differential GPS," *Proc. ION GPS*, 1993.
[82] M. B. El-Arini, J. A. Klobuchar, and P. H. Doherty, "Evaluation of the GPS WAAS ionospheric grid algorithm during the peak of the current solar cycle," *Proc. ION National Technical Meeting*, 1994.
[83] R. Muellerschoen, W. Bertiger, M. Lough, D. Stowers, and D. Dong, "An internet-based global differential GPS system, initial results," *ION GPS*, 2000.
[84] J. A. Klobuchar, "Ionospheric time-delay algorithm for single-frequency GPS users," *IEEE Trans. on Aerospace and Electronic Systems*, no. 3, pp. 325–331, 1987.
[85] T. Fuller-Rowell, "USTEC: A new product from the Space Environment Center characterizing the ionospheric total electron content," *GPS Solutions*, vol. 9(3), pp. 236–239, 2005.
[86] M. B. El-Arini, P. A. O'Donnell, P. M. Kellam, J. A. Klobachar, T. C. Wisser, and P. H. Doherty, "The FAA Wide Area Differential GPS(WADGPS) static ionospheric experiment," *Evolution through Integration of Current and Emerging Systems*, pp. 485–496, 1993.
[87] F. d. S. Prol, P. d. O. Camargo, and M. T. d. A. H. Muella, "Comparative study of methods for calculating ionospheric points and describing the GNSS signal path," *Boletim de Ciências Geodésicas*, vol. 23, no. 4, pp. 669–683, 2017.
[88] C. Chao, "The tropospheric calibration model for Mariner Mars 1971," JPL, Technical Report 19740008870, Mar 01, 1974.
[89] M. Bevis, S. Businger, T. A. Herring, C. Rocken, R. A. Anthes, and R. H. Ware, "GPS meteorology: Remote sensing of atmospheric water vapor using the Global Positioning System," *Journal of Geophysical Research: Atmospheres*, vol. 97 (D14), pp. 15 787–15 801, 1992.
[90] G. Lanyi, "Tropospheric delay effects in radio interferometry," *TDA Prog. Rep. 42-78, vol. April*, pp. 152–159, 1984.
[91] J. Davis, T. Herring, I. Shapiro, A. Rogers, and G. Elgered, "Geodesy by radio interferometry: Effects of atmospheric modeling errors on estimates of baseline length," *Radio Science*, vol. 20(6), pp. 1593–1607, 1985.
[92] A. Niell, "Improved atmospheric mapping functions for VLBI and GPS," *Earth, Planets and Space*, vol. 52(10), pp. 699–702, 2000.
[93] A. Farah, "Accuracy Assessment Study of UNB3m Neutral Atmosphere Model for Global Tropospheric Delay Mitigation," *Artificial Satellites*, vol. 50(4), pp. 201–215, 2015.
[94] K. Kazmierski, M. Santos, and J. Bosy, "Tropospheric delay modeling for the EGNOS augmentation system," *Survey Review*, vol. 49(357), pp. 399–407, 2017.
[95] W. Li, Y. Yuan, J. Ou, H. Li, and Z. Li, "A new global zenith tropospheric delay model IGGtrop for GNSS applications," *Chinese Science Bulletin*, vol. 57(17), pp. 2132–2139, 2012.

APPENDIX

A. WADGNSS

The appendix discusses an example approach for the implementation of Strategy B as defined in Section V-B. The approach is strongly motivated by [32], [33] which document a precursor study leading to WAAS.

WADGNSS Reference Station Processing. Receiver r provides code and carrier phase measurements for each satellite s and frequency f. These measurements are, respectively denoted by $\phi^s_{r,f}$ and $\rho^s_{r,f}$ where the value of f is either $L1$ or $L2$. The models for these measurements are given by eqns. (1–4). The second line of each equation contains the common-mode errors which should be removed by differential processing. All the error terms enter all four equations in an identical manner with the exception of

the ionospheric terms. Also, the number of unknown quantities can be reduced by noting that the two ionospheric delay terms I^s_{L1} and I^s_{L2} in these four equations are both related (to first-order) to the slant total electron count (TEC) along the signal pathway from satellite s to reference station r by the equations

$$I^s_{L1} = \frac{40.3}{f^2_{L1}}\, TEC \quad \text{and} \quad I^s_{L2} = \frac{40.3}{f^2_{L2}}\, TEC. \tag{11}$$

Therefore, the ionospheric delay will be compensated by estimating a parameterized function that maps to TEC, which is then used to compute I^s_{L1} and I^s_{L2} using eqns. (11).

One set of strategies [33], [65]–[71] starts by separating the TEC from the other portions of eqns. (1–4) while also reducing the effects of noise and multipath. Some articles [72]–[74] propose employing the Hatch filter [75]. The approach of Enge *et al.* [33] builds on an idea from [76] by using changes in the carrier measurements to estimate changes in the pseudorange and ionosphere. The changes in carrier measurements

$$\delta\phi^s_{r,f}(n) = \phi^s_{r,f}(n) - \phi^s_{r,f}(n-1) \tag{12}$$

remove the need to estimate the (constant) carrier integer ambiguities which cancel in the time difference as long as there is no loss of phase-lock. The symbol f signifies the measurement frequency which can be $L1$ or $L2$. This dual-frequency carrier-smoothing filter is based on the following observation equation,

$$\begin{bmatrix} \tilde{\rho}^s_{r,L1} \\ \delta\phi^s_{r,L1} \\ \tilde{\rho}^s_{r,L2} \\ \delta\phi^s_{r,L2} \end{bmatrix} \doteq \begin{bmatrix} 1 & 0 & \frac{40.3}{f^2_{L1}} & 0 \\ 0 & 1 & 0 & -\frac{40.3}{f^2_{L1}} \\ 1 & 0 & \frac{40.3}{f^2_{L2}} & 0 \\ 0 & 1 & 0 & -\frac{40.3}{f^2_{L2}} \end{bmatrix} \begin{bmatrix} \bar{\rho}^s_r \\ \delta\bar{\rho}^s_r \\ TEC^s_r \\ \delta TEC^s_r \end{bmatrix} + v^s_r \tag{13}$$

where

$$\bar{\rho}^s_r = R(\mathbf{p}_r, \mathbf{p}^s) + ct_r - ct^s + T^s \tag{14}$$

and v^s_r is a noise vector that accounts for the cumulative effects of multipath and receiver noise, which are both assumed to be zero mean and uncorrelated. The quantity $\delta\bar{\rho}^s_r$ in the right-hand side of eqn. (12) is the change in $\bar{\rho}^s_r$ between two consecutive epochs n and $n-1$:

$$\delta\bar{\rho}^s_r = \bar{\rho}^s_r(n) - \bar{\rho}^s_r(n-1) \tag{15}$$

The ρ quantities on the left-hand side (i.e., $\tilde{\rho}^s_{r,L1}$ and $\tilde{\rho}^s_{r,L2}$) are the calibrated measurements after the receiver and satellite hardware bias estimates have been removed:

$$\tilde{\rho}^s_{r,L1} = \rho^s_{r,L1} - c\hat{b}_{r_{L1,\rho}} + c\hat{b}^s_{L1,\rho} \tag{16}$$

$$\tilde{\rho}^s_{r,L2} = \rho^s_{r,L2} - c\hat{b}_{r_{L2,\rho}} + c\hat{b}^s_{L2,\rho}. \tag{17}$$

Alternative approaches to estimate the ionosphere time delays in the presence of receiver and satellite hardware biases are described in [65]–[71].

For each satellite, eqn. (13) is used as the measurement equation for either least squares or a simple Kalman filter designed to attenuate the effects of noise and multipath. The state vector for each filter includes: $\bar{\rho}^s_r$, $\delta\bar{\rho}^s_r$, TEC^s_r, and δTEC^s_r.

The symbol TEC^s_r in eqn. (13) represents the slant TEC for receiver r and satellite s. This is the cumulative delay experienced by the signal on its non-vertical path through the ionosphere, which is unique for each satellite and receiver. The ionospheric delay map will model the vertical TEC at the ionospheric pierce point of the signal. The conversion of vertical to slant TEC is

$$TEC^s_r = F(E^s_r)\, TEC_v(p^s_{p_r}) \tag{18}$$

by use of the ionospheric obliquity factor $F(E^s_r)$

$$F(E^s_r) = \frac{1}{\sin(E^s_{p_r})} = \frac{1}{\sqrt{1 - \left[\frac{r_e \cos(E^s_r)}{r_e + h_m}\right]^2}} \tag{19}$$

where E^s_r is the elevation angle for satellite s at receiver r, $E^s_{p_r}$ is the local elevation angle at the pierce point $p^s_{p_r}$, r_e is the average radius of the Earth, and h_m is the height of the maximum electron density (assumed to be 350 km). After the slant ionospheric delays for all satellites in view for the reference station have been smoothed and converted to vertical delay estimates, they are sent to the master station for further processing.

The symbol $\bar{\rho}^s_r$ in eqn. (13) represents the *iono-free smoothed pseudorange estimate*. This quantity must be compensated for tropospheric delays before being used to estimate the satellite clock and satellite position error vector. The tropospheric delay is a function of elevation angle, pressure, temperature and humidity (see Chapter 1 of [17]) . The literature provides many models for tropospheric delay estimate [58], [77]–[79]. One of these models (e.g. UNB3M [58]) is implemented and used to compensate the $\bar{\rho}^s_r$ for the predictable portion of tropospheric effects. After compensating for the atmospheric (i.e., ionospheric and tropospheric) delays, smoothed pseudorange are sent to the master station.

WADGNSS Master Station Algorithms. The master station accumulates the data from all base stations for all satellites. It then assembles a vector of the vertical TEC's that it uses to estimate the TEC map as a function of the pierce point $p^s_{p_r}$. Separately it assembles a vector of the atmospheric-free smoothed pseudoranges that it uses to estimate the satellite clock and position error vectors.

Estimation of Ionospheric TEC Grid Map: Each reference station's computed TEC is organized as a vector:

$$\tilde{\mathbf{I}}^S_r = \begin{bmatrix} TEC_r(p^{s_1}_{p_r}) \\ TEC_r(p^{s_2}_{p_r}) \\ \vdots \\ TEC_r(p^{s_M}_{p_r}) \end{bmatrix} \tag{20}$$

In this document, for simplicity of notation, we assume that there are total M satellites in view from all reference stations.

The master station receives the TEC vectors $\tilde{\mathbf{I}}_r^S$ from N reference stations, so $r = 1,\ldots,N$. This reference station data is concatenated to form a large measurement vector,

$$\tilde{\mathbf{I}}^S = \begin{bmatrix} \tilde{\mathbf{I}}_{r_1}^S \\ \tilde{\mathbf{I}}_{r_2}^S \\ \vdots \\ \tilde{\mathbf{I}}_{r_N}^S \end{bmatrix} \doteq \mathbf{I}^S + \boldsymbol{\varepsilon}^S \tag{21}$$

which is interpreted as the true ionospheric delay vector $\mathbf{I}^S$ plus a measurement error vector $\boldsymbol{\varepsilon}^S$. The vector of measurements $\tilde{\mathbf{I}}^S$ will be used to maintain a vertical TEC map function.

The vertical TEC map is constructed using a grid of vertical TEC values denoted by the vector $\mathbf{I}^G$ [80]–[82]. The value of the k-th element of $\mathbf{I}^G$ represents the vertical TEC at a pierce point p_{p_k}. The set of points $\{p_{p_k}\}_{k=1}^K$ forms a regular grid. The vertical TEC at an arbitrary pierce point p_p within the geographical extent of the grid points is computed as a linear function of the values at the grid points:

$$TEC_v(p_p) \;=\; \mathbf{w}(p_p)\,\mathbf{I}^G \tag{22}$$

where $\mathbf{w}(p_p)$ is a vector of weights. The k-th element of the weight vector $w_k = [\mathbf{w}(p_p)]_k$ shows how much the vertical TEC value $[I^G]_k$ at the k-th grid point p_{p_k} contributes to the value of the TEC at the desired pierce point p_p.

The elements of $\mathbf{w}(p_p) = [w_1,\ldots,w_K]$ should satisfy a few constraints. The first constraint is that $\sum_{i=k}^K w_k = 1$, so that eqn. (22) interpolates the value for $TEC(p_p)$ from the TEC values at the grid points. A second constraint is that when $p_p = p_{p_k}$ the vector $\mathbf{w}(p_{p_k})$ should be all zero except for a single one as the k-th element. This causes $TEC(p_p)$ to evaluate to match the k-th element of the vector $\hat{\mathbf{I}}^G$. A third constraint is that the k-th element $[\mathbf{w}(p_p)]_k$ should decrease smoothly as $d_k = \|p_p - p_{p_k}\|$ increases. This results in a smooth interpolation between the grid point values. One example choice of the weighting function is the inverse distance approach [33], where the weights are selected as

$$a_k = 1/d_k \text{ and } w_k = \frac{a_k}{\sum_{i=1}^K a_i}$$

which requires special treatment for the case where $d_k = 0$.

The vector of measurements $\tilde{\mathbf{I}}^S$ defined in eqn. (21) will be used to estimate the TEC values at the grid points (i.e., $\mathbf{I}^G$). The i-th element of $\tilde{\mathbf{I}}^S$ corresponds to a pierce point p_{p_i}. For accurate estimation of the TEC map, this set of pierce points should be well distributed throughout the geographic region defined by the grid points. Using eqn. (22) allows calculation of a weight matrix $\mathbf{W}$ with rows defined by $\mathbf{w}(p_{p_i})$ such that the measurements relate to the grid values as

$$\tilde{\mathbf{I}}^S \doteq \mathbf{W}\,\mathbf{I}^G + \boldsymbol{\varepsilon}^S. \tag{23}$$

The value of $w_{i,k} = [\mathbf{W}]_{i,k}$ is the element in the i-th row of the k-th column of matrix $\mathbf{W}$, which represents the interpolation weight from the k-th grid point at the i-th pierce point.

If the spatial distribution of the pierce points results in the matrix $\mathbf{W}$ being full column rank, then eqn. (23) could be solved as

$$\hat{\mathbf{I}}^G \doteq (\mathbf{W}^T\mathbf{W})^{-1}\,\mathbf{W}^T\,\tilde{\mathbf{I}}^S. \tag{24}$$

Alternatively, either constraints could be added to ensure that a unique and smooth solution exists or eqn. (23) could be used as the measurement equation for a Kalman filtering approach to allow information accumulation and noise reduction over time [41].

Estimation of Satellite Orbit and Clock Corrections: The satellite orbit and clock correction vectors are estimated by the master station using the atmospheric-free smoothed pseudorange vectors from all reference base stations.

Based on eqn. (14), the atmospheric-free smoothed pseudorange between reference station r to satellite s is

$$\bar{\rho}_r^s \doteq R(\mathbf{p}_r,\mathbf{p}^s) + ct_r - ct^s + w_r^s. \tag{25}$$

This measurement is based on the actual satellite position, not the computed satellite position using on the ephemeris data. These two items are related to each other by $\mathbf{p}^s = \hat{\mathbf{p}}^s + \delta\mathbf{p}^s$ where $\hat{\mathbf{p}}^s$ is the calculated satellite location and $\delta\mathbf{p}^s$ is satellite position error vector.

The range can be equivalently represented as a dot product

$$\begin{aligned} R(\mathbf{p}_r,\mathbf{p}^s) &= \mathbf{e}_r^s \cdot [(\hat{\mathbf{p}}^s + \delta\mathbf{p}^s) - \mathbf{p}_r] \\ &= \mathbf{e}_r^s \cdot \delta\mathbf{p}^s + \mathbf{e}_r^s \cdot (\hat{\mathbf{p}}^s - \mathbf{p}_r) \end{aligned} \tag{26}$$

where $\mathbf{e}_r^s = \frac{\mathbf{p}_r - \mathbf{p}^s}{\|\mathbf{p}_r - \mathbf{p}^s\|}$ is the unit vector from satellite s to reference station r; and w_r^s is the atmospheric-free smoothed pseudorange estimation error. Since the quantity $(\hat{\mathbf{p}}^s - \mathbf{p}_r)$ is known for the reference sations, it can be removed by defining a new variable

$$y_r^s = \bar{\rho}_r^s - \mathbf{e}_r^s \cdot (\hat{\mathbf{p}}^s - \mathbf{p}_r). \tag{27}$$

Combining the above equations yields the measurement model

$$y_r^s \doteq \mathbf{e}_r^s \cdot \delta\mathbf{p}^s + ct_r - ct^s + w_r^s. \tag{28}$$

where $r = 1,\ldots,N$ counts over reference stations and $s = 1,\ldots,M$ counts over GNSS satellites.

The master station will estimate the vector

$$\mathbf{x} = \begin{bmatrix} \delta\mathbf{p}^T & \mathbf{B}^T & \mathbf{b}^T \end{bmatrix}^T, \tag{29}$$

where for $\delta\mathbf{p}^s \in \Re^3$

$$\begin{aligned} \delta\mathbf{p} &= \begin{bmatrix} (\delta\mathbf{p}^1)^T & (\delta\mathbf{p}^2)^T & \ldots & (\delta\mathbf{p}^M)^T \end{bmatrix}^T \in \Re^{3M}, \\ \mathbf{B} &= \begin{bmatrix} ct^1 & ct^2 & \ldots & ct^M \end{bmatrix}^T \in \Re^M, \\ \mathbf{b} &= \begin{bmatrix} ct_1 & ct_2 & \ldots & ct_N \end{bmatrix}^T \in \Re^N. \end{aligned}$$

Using this definition of $\mathbf{x}$ and eqn. (28), the vector of measurements for the m_r satellites at reference station r, denoted as $\mathbf{y}_r$, can be organized as

$$\mathbf{y}_r \doteq \begin{bmatrix} \mathbf{E}_r & -\mathbf{I}_r & \mathbf{1}_r \end{bmatrix}\mathbf{x} + \mathbf{w}_r. \tag{30}$$

The matrix $\mathbf{E}_r \in \Re^{m_r \times (3M)}$ is compose of rows that are all zeros, with the exception that in each row, where the i-th row corresponds to $y_r^{s_i}$, the row vector $\mathbf{e}_r^{s_i}$ will be in the columns corresponding to $\delta \mathbf{p}^{s_i}$. The matrix $\mathbf{I}_r \in \Re^{m_r \times M}$ is composed of rows that are all zeros with the exception that in the i-th row corresponding to $y_r^{s_i}$ there is a one in the column corresponding to ct^{s_i}. The matrix $\mathbf{1}_r \in \Re^{m_r \times N}$ is composed of rows that are all zeros with the exception that in each row there is a one in the column corresponding to ct_r. For example, if reference station $r = 3$ was receiving satellites 1 and 4, then

$$\mathbf{E}_3 = \begin{bmatrix} (\mathbf{e}_r^1)^T & \mathbf{0} & \mathbf{0} & \mathbf{0} & \mathbf{Z}_{3(M-4)} \\ \mathbf{0} & \mathbf{0} & \mathbf{0} & (\mathbf{e}_r^4)^T & \mathbf{Z}_{3(M-4)} \end{bmatrix},$$

$$\mathbf{I}_3 = \begin{bmatrix} \mathbf{1} & \mathbf{0} & \mathbf{0} & \mathbf{0} & \mathbf{Z}_{M-4} \\ \mathbf{0} & \mathbf{0} & \mathbf{0} & \mathbf{1} & \mathbf{Z}_{M-4} \end{bmatrix},$$

$$\mathbf{1}_3 = \begin{bmatrix} \mathbf{0} & \mathbf{0} & \mathbf{1} & \mathbf{0} & \mathbf{0} \\ \mathbf{0} & \mathbf{0} & \mathbf{1} & \mathbf{0} & \mathbf{0} \end{bmatrix},$$

where $\mathbf{Z}_p \in \Re^{1 \times p}$ is a row vector with all zeros. The matrix $\mathbf{1}_3$ consists of all zeros except the third column that is 1.

Concatenating the measurements from all the reference stations provides a measurement equation of the form

$$\mathbf{y} \doteq \mathbf{H}\mathbf{x} + \mathbf{w} \tag{31}$$

where

$$\mathbf{y} = \begin{bmatrix} \mathbf{y}_1 \\ \mathbf{y}_2 \\ \vdots \\ \mathbf{y}_N \end{bmatrix}, \quad \mathbf{H} = \begin{bmatrix} \mathbf{E}_1 & -\mathbf{I}_1 & \mathbf{1}_1 \\ \mathbf{E}_2 & -\mathbf{I}_2 & \mathbf{1}_2 \\ \vdots & \vdots & \vdots \\ \mathbf{E}_N & -\mathbf{I}_N & \mathbf{1}_N \end{bmatrix}, \text{ and } \mathbf{w} = \begin{bmatrix} \mathbf{w}_1 \\ \mathbf{w}_2 \\ \vdots \\ \mathbf{w}_N \end{bmatrix}.$$

The master station can solve eqn. (31) by a variety of methods (e.g., batch least squares). If there are more measurements than unknowns in the WADGNSS network, the system of equations is over-determined. The least squares solution is

$$\hat{\mathbf{x}} = (\mathbf{H}^T\mathbf{H})^{-1}\mathbf{H}^T\mathbf{y}. \tag{32}$$

It is also possible through suitable parameterizations to extract information from multiple epochs of data using recursive least squares or Kalman filter methods.

WADGNSS Reference Network Design Constraints: In (31), if m represents the minimum number of satellites available per base station, then there will be at least Nm measurements and $4M + (N-1)$ unknowns[1]. To achieve an over-determined set of equations requires

$$Nm \geq 4M + (N-1) \tag{33}$$

Therefore, at least

$$N \geq \frac{4M-1}{m-1}$$

reference stations are required. For $M = 32$ and $m = 6$, at least $N = 26$ reference stations would be required. In addition, the reference stations must be geographically distributed such that the matrix $\mathbf{H}$ is full column rank and well-conditioned.

B. Real-time PPP Approach

Appendix A described an implementation approach for WADGNSS. Many entities (IGS, JPL, WAAS) have investigated and established WADGNSS systems [30]–[34], [83]. Various services now provide real-time access to the products of their WADGNSS: TEC maps, satellite position and clock corrections, and satellite inter-frequency biases. These services enable real-time Precise Point Positioning (PPP).

This appendix discusses data sources and methods for computing: satellite orbit corrections and precise ephemeris; satellite clock corrections; ionospheric corrections; tropospheric corrections; and satellite hardware bias corrections. It also summarizes reported accuracy for each.

Satellite and Clock Orbit Corrections. Satellite ephemeris/orbit error is the difference between the satellite's true position p^s and the position $\hat{p}^s$ computed using ephemeris data. This error develops is due to uncertainty in the gravitational model, inaccuracy of the orbit representation and inadequately modeled surface forces on the satellites (e.g., solar radiation, particles of the Earths atmosphere and air drag).

Although GPS satellites have stable atomic clocks, all clocks drift relative to each other. The main distinction of higher quality clocks is that they drift more slowly, yet it is not possible to maintain synchronization of the satellite clocks with GPS time, which results in satellite clock biases. The navigation message provides parameters to predict the clock biases $c\hat{t}^s(t)$, but there will still be residual clock biases $c\delta t^s(t)$ that range from 1-3 meters.

Satellite Orbit: Data Sources and Reported Accuracy: IGS has been working on establishing precise orbit and clock correction service since 1990. Currently the service provides multiple versions of these corrections. Table VIII provides a description of the different data products for orbit and clock corrections. It includes communication period, reported accuracy, and latency information.

Satellite Orbit: Computations: The satellite position $\hat{\mathbf{p}}^s(t)$ and velocity vectors $\dot{\hat{\mathbf{p}}}^s(t)$ in ECEF frame are computed from the broadcast ephemeris. For the IGS-RTS service, the satellite orbit correction parameters $\delta\mathbf{O}_0$ and rate $\delta\dot{\mathbf{O}}_0$ are provided in Antenna Phase Center coordinates (i.e., APC frame) along with a reference time t_0 every 60 seconds. Given these items, the correction computation involves four steps [52]:

1) The satellite orbit correction parameters $\delta\mathbf{O}_0$ and rate $\delta\dot{\mathbf{O}}_0$ are provided every 60 seconds along with a reference time t_0. The orbit correction at any time t is computed as

$$\delta\mathbf{O}(t) = \delta\mathbf{O}_0 + \delta\dot{\mathbf{O}}_0\,(t - t_0). \tag{34}$$

[1]The $(N-1)$ appears instead of N because clock errors can be estimated only relative to a fixed reference. Therefore, one of the values can be set to an arbitrary value such as zero.

TABLE VIII: IGS product for precise satellite orbit and clock correction:

Product	Communicaton period		Accuracy		latency
	Orbit	Sat. Clock	Orbit	Sat.Clock	
Real-time	5-60 sec	5 sec	5.0 cm	300 ps	25 sec
Ultra-Rapid (Predicted Half)	15 min	15 min	5.0 cm	3 ns	predicted
Ultra-Rapid (Observed Half)	15 min	15 min	3.0 cm	150 ps	3-9 hrs
Rapid	15 min	5 min	2.5 cm	75 ps	17-41 hrs
Final	15 min	30 sec	2.0 cm	75 ps	12-18 days

In APC-frame, the vector $\delta\mathbf{O} = \begin{bmatrix}\delta O_r & \delta O_a & \delta O_c\end{bmatrix}^\top$ has radial, along-track, and cross-track components.

2) The radial $\mathbf{e}_r$, along $\mathbf{e}_a$, and cross-track $\mathbf{e}_c$ unit vectors in the ECEF frame are computed as

$$\mathbf{e}_a = \frac{\dot{\hat{\mathbf{p}}}^s}{\|\dot{\hat{\mathbf{p}}}^s\|},\ \mathbf{e}_c = \frac{\hat{\mathbf{p}}^s \times \dot{\hat{\mathbf{p}}}^s}{|\hat{\mathbf{p}}^s \times \dot{\hat{\mathbf{p}}}^s|},\ \mathbf{e}_r = \mathbf{e}_a \times \mathbf{e}_c. \tag{35}$$

3) The orbit correction $\delta\mathbf{O}(t)$ is transformed from APC frame to ECEF frame as

$$\delta\mathbf{p}^s(t) = \begin{bmatrix}\mathbf{e}_r & \mathbf{e}_a & \mathbf{e}_c\end{bmatrix} \delta\mathbf{O}(t). \tag{36}$$

4) The precise orbit $\hat{\mathbf{p}}^{s_p}$ is computed as

$$\hat{\mathbf{p}}^{s_p}(t) = \hat{\mathbf{p}}^s(t) - \delta\mathbf{p}^s(t). \tag{37}$$

After the computation of precise orbit $\hat{\mathbf{p}}^{s_p}(t)$, it can be used in two ways that are nearly the same. First, for a user with access to the receiver navigation code, the precise satellite location can be used for computing the estimated range $R(\hat{\mathbf{p}}_r, \hat{\mathbf{p}}^{s_p}) = \|\hat{\mathbf{p}}_r - \hat{\mathbf{p}}^{s_p}\|$ and satellite-to-receiver unit vector. Second, for a user supplying corrections to a receiver, the receiver will still use $\hat{\mathbf{p}}^s$, the ephemeris portion of the corrections $\hat{E}^{s_p}$ would be

$$\hat{E}^{s_p} = \frac{(\hat{\mathbf{p}}_u - \hat{\mathbf{p}}^{s_p})}{\|\hat{\mathbf{p}}_u - \hat{\mathbf{p}}^{s_p}\|} (\hat{\mathbf{p}}^s - \hat{\mathbf{p}}^{s_p}) \tag{38}$$

where $\hat{\mathbf{p}}_u$ is the approximate user location.

Satellite Clock Computation: IGS-RTS data products provide satellite clock corrections using three polynomial parameters (a_{c_0}, a_{c_1}, a_{c_2}) and the message reference time is t_0. As shown in Table VIII, these parameters are sent every 5 seconds. The correction at time t is computed using the following equation [52]:

$$c\delta t^s(t) = a_{c_0} + a_{c_1}(t - t_0) + a_{c_2}(t - t_0)^2. \tag{39}$$

The clock correction $c\delta t^s(t)$ is computed in meters. The equation for the precise satellite clock ct^{s_p} is

$$ct^{s_p}(t) = ct^s(t) + c\delta t^s(t). \tag{40}$$

Ionosphere Error Mitigation. The amount of ionospheric delay incurred by a GNSS signal depends on the number of free electrons or ions existing along the signal path. This measure is referred to as the Total Electron Content (TEC) which is measured in Total Electron Content Units (TECU's), where $1\ TECU = 1\times10^{16}\ TEC$ means there are 1×10^{16} electrons in a $1\,m^2$ cylinder around the signal path. This delay is dependent on the frequency of the carrier signal; therefore, it can be measured and removed by a user with a multi-frequency receiver. In a network GNSS approach measurements from across the network can be combined to calibrate a TEC map, as described in Appendix A. A single frequency receiver cannot calibrate the ionospheric delay itself, but can incorporate ionospheric models from external sources.

Data Sources and Reported Accuracy. Table IX summarizes a few example ionospheric delay map products [37]. The table includes reported accuracy, sampling period, map resolution and product latency. Some frequently used ionospheric delay products are:

- **Klobuchar Model:** The ionospheric delay model that is available to all GPS users as part of the broadcast navigation message is the Klobuchar model [84]. The modeling effort included an assessment of expected accuracy versus the number of coefficients. The broadcast model uses 8 coefficients to achieve for 50% correction accuracy goal. Increasing this number of coefficients would only remove 70% to 80% RMS of the ionospheric effects.
- **Global Ionosphere Maps (GIM):** GIM represents a tool to monitor global ionospheric patterns. It provides the instantaneous snapshots of the global TEC distribution [34]. This product was developed by IGS Ionosphere Working Group (Iono-WG) established on May 1998. Currently four IGS Ionosphere Associate Analysis Centers (IAACs) provide data to generate GIMs on a daily basis. GIM produces a 2-dimensional ionosphere TEC map that corresponds to a 450 km ionospheric shell height. The IGS final GIMs are provided in Ionosphere Map Exchange (IONEX) format.
- **US Total Electron Content (US-TEC):** USTEC is a service that distributes a TEC map for the USA. The product was developed through a collaboration between the Space Weather Prediction Center (SWPC), the National Geodetic Survey (NGS), the National Centers for Environmental Information (NCEI), and the Global Systems Division (GSD) [53], [85].

Methodology: For single-frequency real-time users in North America, US-TEC is the most suitable ionospheric delay product. US-TEC (and other services) provides vertical TEC values for a uniform grid of point locations at a specified broadcast interval which can extend from minutes to hours (see Table IX). The user computes a TEC value for its specific location by interpolating between the provided values in both space and time [86]. Linear temporal interpolation is sufficient. Spatial interpolation can be

TABLE IX: Ionospheric Delay Map Products.

Product	Reported accuracy, TECU	Broadcast interval	Latency	Resolution	
				longitude, deg	latitude, deg
IGS Final Ionospheric TEC Grid	2-8	2 hours	11 days	5	2.5
IGS Rapid Ionospheric TEC Grid	2-9	2 hours	$\leq$ 24 hours	5	2.5
US-TEC	2.4	15 min	Real-time	1	1

performed in different ways. Given the values of the vertical TECU values at the grid points, linear spatial interpolation approaches take the form of eqn. (22):

$$\widehat{TEC}_v(\mathbf{p}^s_{p_u}) = w((\mathbf{p}^s_{p_u})\hat{\mathbf{I}}^G. \tag{41}$$

This interpolation is based on the pierce point $\mathbf{p}^s_{p_u}$, which the user computes using the satellite and receiver locations [87]. The discussion in Appendix A includes an example distance weighted approach. Spatial interpolation provides the vertical total electron count at the pierce point, which is converted to slant delay using eqns. (11) and (18):

$$\hat{I}^s_{L1} = \frac{40.3}{f^2_{L1}}\ F(E^s_r)\ \widehat{TEC}_v(\mathbf{p}^s_{p_r}) \tag{42}$$

Troposphere Error Mitigation. The troposphere is the lowest layer of the atmosphere extending to about 50 km above the surface of Earth. It is a non-ionized and non-dispersive medium, so usage of multiple frequency measurements cannot eliminate tropospheric delay. This delay is affected by satellite elevation angle, receiver altitude, atmospheric temperature, pressure and humidity. The tropospheric delay can be divided into two parts: the dry/hydrostatic part and the wet part. About 90% of the total tropospheric delay is contributed by the dry component and 10% by the wet component.

Standard tropospheric delay models for satellite measurement T^s have the form:

$$T^s = d^s_{dry}\ \ M^s_{dry}\ +\ d^s_{wet}\ \ M^s_{wet}. \tag{43}$$

The symbols d^s_{dry} and d^s_{wet} are the tropospheric Zenith Path Delay (ZPD) caused by the dry and wet components, respectively. The symbols M^s_{dry} and M^s_{wet} are the mapping functions that convert the ZPD dry and wet components from zenith (or vertical) to slant delays based on satellite elevation at the user location.

Literature and Reported Accuracy: The literature contains a variety of ZPD models, for example: Hopfield [77], Saastamoinen [78]. These models depend on various atmospheric parameters: receiver altitude, temperature, pressure, and humidity. Therefore, local sensors (e.g., barometer, hygrometer, thermistor) are necessary to compute tropospheric delay accurately from these models. In addition to tropospheric ZPD, there are also many mapping functions to compute slant tropospheric delay: Chao [88], Herring [89], Lanyi [90], Davies [91] and Niell mapping functions [92].

Recently, several entities have proposed newer hybrid tropospheric models combining a ZPD model and mapping function [58], [79] that do not require additional sensors; instead, additional lookup tables are provided for computing typical atmospheric parameters (i.e., temperature, pressure and humidity) for a specific location at a specific date and time. Example models are: UNB [58], UNB3M [93], EGNOS [94], and IGGtrop [95]. Different characteristics of these models are summarized in Table X, based on information from [79].

Description of UNB3M: For this research project, the UNB3M model was selected as it is specifically designed for users in North America. The UNB model has been developed by researchers of University of New Brunswick, Canada [58]. The model consists of the Saastamoinen zenith delay model, the Niell mapping functions, and a look-up table to compute predicted values for temperature, pressure and water vapor pressure varying with respect to date, time, latitude and height. UNB3M model is the modified version of UNB model. In this model, instead of water vapor pressure the look-up table contains relative humidity. The model computes dry and wet delay components using look-up table values and Niell mapping functions.

Satellite Hardware Bias. The measurement models in eqns. (1-4) and the WADGNSS approach is Appendix A did not account for delays due to satellite hardware that may be different for code, phase, or different frequencies. These delays, referred to as satellite hardware biases or Differential Code Biases (DCB), can be as large as 12 nanoseconds. This bias are constant unless there is a satellite hardware substitution. The biases can be estimated in a network WADGNSS approach or can be downloaded from various sources.

Data Sources: Two sources for the DCB parameters are:

- The Crustal Dynamics Data Information System provides the DCB in MGEX data format. The file can be found at the URL: "ftp://cddis.nasa.gov/gnss/products/bias/".
- IGS-RTS provides the DCB as a message in RTCM format [36].

Methodology: For the L1 C/A pseudorange measurement the satellite DCB $cb^s_{L1,\rho}$ is:

$$cb^s_{L1,\rho} = -T_{GD} + ISB_{C1,P1} \tag{44}$$

where $ISB_{C1,P1}$ is the delay of L1 C/A signal with respect to L1 P signal and T_{GD} is the group delay parameter in the navigation message. The group delay represents the time difference from generation to transmission of the P signal.

TABLE X: Tropospheric Delay Model Accuracy.

Model	UNB	UNB3M	EGNOS	IGGtrop
Accuracy (cm)	6-10	5.4	5.7	4.4
Location	North America	North America	Europe	Global